Solar Energy Materials & Solar Cells 107 (2012) 87–111

Contents lists available at SciVerse ScienceDirect

Solar Energy Materials & Solar Cells

journal homepage: www.elsevier.com/locate/solmat

Review

Organic—inorganic hybrid solar cells: A comparative review

Matthew Wright *, Ashraf Uddin

ARC Photovoltaics Centre of Excellence, University of New South Wales, Sydney, NSW 2052, Australia

ARTICLE INFO

Article history:
Received 21 February 2012
Received in revised form
30 June 2012
Accepted 9 July 2012
Available online 4 September 2012

Keywords:
Hybrid solar cell
Bulk-heterojunction
Inorganic acceptor
Limitations
Surface modification

ABSTRACT

Organic materials have recently become of great interest for photovoltaic applications, due to their potential to utilise high throughput, solution phase processing, which will lead to low cost electricity production. Hybrid solar cells combine organic and inorganic materials with the aim of utilising the low cost cell production of organic photovoltaics (OPV) as well as obtaining other advantages, such as tuneable absorption spectra, from the inorganic component. Whilst hybrid solar cells have the potential to achieve high power conversion efficiencies (PCE), currently obtained efficiencies are quite low. The design of the inorganic material used as the electron acceptor in hybrid solar cells, particularly the electronic structure, is crucial to the performance of the device. There exists an optimal electronic structure design for an inorganic acceptor. To date, four major material types have been investigated, being cadmium compounds, silicon, metal oxide nanoparticles and low band gap nanoparticles. Currently, Cadmium Sulfide (CdS) quantum dots represent the state of the art, yielding a PCE of greater than 4%. This review compares the electronic structure of these materials with the optimal design components of an inorganic material and also explores possible limitations to the PCE of these devices, such as nanomorphology control and nanoparticle surface chemistry. This report provides the reader with a concise synthesis of the current state of the art for bulk heterojunction organic—inorganic hybrid solar cells. Additionally, it highlights key research areas which require attention to allow for the commercialisation of this technology.

Contents

* Corresponding author. Tel.: +61 2 9385 9827; fax: +61 2 9385 5104.
E-mail address: matthew.wright@unsw.edu.au (M. Wright).

0927-0248/$ - see front matter © 2012 Elsevier B.V. All rights reserved.
http://dx.doi.org/10.1016/j.solmat.2012.07.006

1. Introduction

Projected increases in world energy demand and increasing global concern over the issue of climate change have focussed research attention on renewable, clean energy sources, of which photovoltaics (PV) is a promising example. Silicon solar cells currently dominate the PV market, as they have demonstrated high power conversion efficiencies (PCE), up to 25% [1], due to the excellent charge transport properties and environmental stability of high purity silicon. The PV industry has displayed rapid growth in recent times; however, higher energy costs, when compared to traditional generation methods, have thus far prevented PV from supplying a significant portion of the world's stationary energy [2,3]. The methods used to manufacture high efficiency silicon solar cells are costly. Purification techniques used to produce high quality silicon, coupled with high temperature, low throughput manufacturing techniques lead to high energy costs, which is hindering the progress of PV. A possible alternative to crystalline silicon solar cells comes in the form of inorganic thin film devices. In these devices, a desirable trade-off can be made between the reduced thickness of the semiconducting layer (reducing cost) and an inevitable reduction in efficiency, due to the limited crystalline quality of the thin film. Current compounds used for this technology include Cu(In,-Ga)Se_2 and Cadmium Telluride (CdTe) [4,5]. Although these devices may provide cost benefits, their production requires the use of very rare materials. Significant impact on the PV industry is yet to be accomplished by this particular technology.

The search for low cost photovoltaics has led researchers to organic materials as possible candidates. The discovery of organic materials which have both conducting and semiconductor properties has led to new and exciting possibilities in the field of optoelectronic devices [6]. The main advantage of organic materials is the ability to produce photovoltaic devices using solution phase techniques, such as ink jet printing or various roll to roll techniques, which could lead to very cheap, high throughput manufacturing [7,8]. The potential speed and simplicity of organic photovoltaics (OPV) processing is unmatched by other current technologies. Additionally, organic semiconductors have very high absorption coefficients [9], which allow very thin films to be used, whilst still absorbing a sufficient portion of the solar spectrum. This reduction in material used, coupled with low cost manufacturing techniques, implies that organic semiconductors have the potential to make a significant impact on the PV market. Extensive research over the last 5 years has produced marked increases in the efficiency of OPV devices [10–13], with the current record certified PCE being 10% [1]. This efficiency has been seen as a landmark milestone since the beginning of research in organic based photovoltaics. Persistent, rapid improvement over the past 12 months would suggest that this 10% milestone is soon to be surpassed. Utilisation of these advantages and recent significant increases in efficiency has led to the production of some preliminary commercial OPV products. Additionally, a few public demonstration projects have been recently undertaken, with the aim of assessing the viability of OPV products in real world settings [14,15].

Organic—inorganic hybrid solar cells combine organic (normally conjugated polymers) and inorganic nanoparticles, with the intent of incorporating the advantages associated with both material groups [16,17]. The inorganic electron acceptor material can provide further advantages to the system, whilst still maintaining low cost processability. First, inorganic acceptor materials are more environmentally stable than organic materials [18]. Adding these materials to OPV devices could assist in overcoming one of the major downfalls of the technology, which is the photo induced degradation of the conjugated organic semiconductors. Second, photogeneration of charge carriers can be achieved by excitons absorbed in the inorganic material [19,20]. The contribution of light absorption by an inorganic acceptor has the potential to be greater than the absorption contribution of PCBM in OPV devices [21,22]. Additionally, quantum confinement, as a result of modification of the size and shape of the inorganic nanoparticle, alters the band gap and thus absorption profile of the nanoparticle [23]. This provides the possibility of choosing the spectral window of the complementary absorption profile [24]. Third, inorganic quantum dots are known for ultrafast photo induced charge carrier transfer to organic semiconductors. This transfer rate has been observed in the order of picoseconds [25]. As this transfer rate is faster than the competing recombination mechanisms, efficient charge transfer between the donor and acceptor can be established. Lastly, the physical dimensions of some inorganic semiconductors, namely oxides, can be tailored via synthesis methods to produce vertically well-aligned nanostructures [26]. This can lead to device architectures which allow simultaneously efficient excitonic dissociation and electron transporting pathways. These advantages could be obtained, whilst maintaining the solution processability and thus high throughput, low cost device production. Although there are multiple theoretical advantages associated with using an inorganic electron acceptor, the currently achieved device efficiencies of hybrid solar cells are significantly lower than polymer:fullerene OPV devices. There exist multiple factors responsible for this discrepancy. Seemingly, the most important issues are related to the nanoparticle surface chemistry and the nanomorphology of the photoactive layer. These two important factors are examined within this review. The key purpose of this article is to introduce the reader to the concept of hybrid organic—inorganic solar cells and to explore the inorganic materials which could produce high performance organic–inorganic hybrid solar cells.

The first section introduces the reader to the concept of hybrid solar cells, detailing the device fabrication and operating characteristics. The main focus of this review is a detailed investigation of the materials used for these solid state devices. In Section 3, ideal characteristics of both donor and acceptor materials are explored and a comprehensive list of material combinations previously examined is presented. These material choices are then analysed and limitations for hybrid solar cells are presented. The final section looks at new characterisation techniques which may help elucidate a deeper understanding of how these devices operate, which is required for efficient device optimisation. The conclusion

provides a future outlook for this technology. It also describes current understanding of commercial aspects for this technology, by highlighting initial existing investigations, which have recently emerged. It then draws attention to important areas of research for the future.

2. Device structure and general operating principles

The device fabrication and operation of hybrid solar cells is very similar to that of organic solar cells, the only difference being that the organic electron accepting material of PCBM (or other fullerene derivatives) is replaced by an inorganic nanoparticle. This could be in the form of quantum dots dispersed in a polymer matrix, or a more complex shaped nanoparticle like nanorods, nanowires or tetrapods, mixed with a polymer. Fig. 1 displays TEM images of CdSe nanoparticles in the form of (a) quantum dots, (b) nanorods and (c) tetrapods [27].

The vast majority of hybrid solar cell devices are planar in nature, consisting of a photoactive layer wedged between two electrodes of different work functions. The device is built on a transparent substrate, usually glass or PET. This substrate may be flexible. The anode consists of a semitransparent oxide layer, usually indium tin oxide (ITO). Its role is to allow light to pass through, and to collect holes from the device. A layer of the conductive polymer mixture (PEDOT–PSS) may be applied between the anode and the photoactive layer. This thin layer is spin coated on top of the ITO surface. The PEDOT–PSS layer serves several functions. As well as a hole transporting layer and exciton blocker, it smooths the ITO surface, seals the active layer from oxygen, and prevents the cathode material from diffusing into the active layer, which can lead to unwanted trap sites [28]. The light absorbing photoactive layer containing the donor and acceptor material is sandwiched between two electrodes. For lab devices, this layer is spin coated from a common solution which contains the polymer donor and inorganic nanoparticles suspended in an appropriate solvent or mixture of solvents. Alternatively, the inorganic acceptor may be grown into a desired shape via multiple synthetic methods. The cathode is usually aluminium, although calcium or magnesium is sometimes used. The function of the cathode is to collect electrons from the device. This layer is deposited via thermal evaporation. With this device structure, the light is illuminated through the glass substrate.

2.1. Structure of photoactive layer

As the fundamental properties of organic semiconductors are different to that of their inorganic counterparts, the operation of OPV devices is different to that of silicon solar cells. In a silicon solar cell, an incident photon breaks a covalent bond, which forms an electron–hole pair. Due to the crystalline nature of the silicon lattice, these charge carriers experience only a small force of interaction. As a result, absorption in silicon leads to effectively free charge carriers. Due to the low relative dielectric constant of organic semiconductors ($\varepsilon_r = \sim 3$) [29,30], there exists a large electrostatic force between electrons and holes. When light strikes the photoactive layer, an excited state is formed; however, the electron and hole are coulombically bound. This bound electron–hole pair is referred to as an 'exciton'. A force is required to overcome this excitonic binding energy so that free charge carriers can be produced and transported throughout the device. In hybrid solar cells, excitons formed in the donor material are dissociated at the donor–acceptor (D–A) interface. The force required to overcome the exciton binding energy is provided by the energy level offset of the lowest unoccupied molecular orbital (LUMO) of the donor and the conduction band edge of the acceptor materials. Fig. 2(a) displays a simplified energy band diagram. This energy offset used to dissociate excitons is denoted as ΔE_{ES} in Fig. 2(a), which is the excited state energy offset. For dissociation of excitons formed in the acceptor material, the energy offset of the highest occupied molecular orbital (HOMO) of the donor and the valence band edge of the acceptor materials is required. This energy offset used to dissociate excitons is denoted as ΔE_{GS} in Fig. 2(a). This is the ground state energy offset. Excitonic dissociation due to this energy offset occurs at the interface between the donor and acceptor phase, and thus, the arrangement of the two materials in the active layer is crucial for the successful operation of the device. Due to the small excitonic diffusion length in conjugated polymers ($\sim$10 nm) [31–33], bi layer structures are severely limited in excitonic dissociation, as there exists only one interface. The only place where dissociation can occur is at the single interface between the materials, implying that only photoexcitation which occurs within an excitonic diffusion length of the interface can produce free charge carriers. In order to increase the interfacial area and thus excitonic dissociation, the donor and acceptor material can be intimately mixed, forming what is called a bulk heterojunction device structure [34]. A comparison of the two heterojunction designs is displayed in Fig. 2b). A device with a large dispersion of interfaces throughout the photoactive layer requires smaller exciton diffusion distances, and thus, a larger exciton dissociation yield is achieved. There exists a trade-off between increasing interfacial area via the intimate dispersion of phases and the creation of efficient conductive pathways through which free electrons and holes may be transported. The arrangement of donor and acceptor phase is thus crucial to device performance.

2.2. Device operation

When a photon is absorbed in the donor material, an exciton is created. This can be dissociated at a D–A interface. Once separated, the electron can transfer to the acceptor material at an interface and be transported to the cathode for charge collection. The hole produced in the donor material travels throughout the polymer and is collected at the anode. This process is displayed as (a) in Fig. 3. The inorganic acceptor material may also contribute useful photocurrent. When light is absorbed in the acceptor material, an

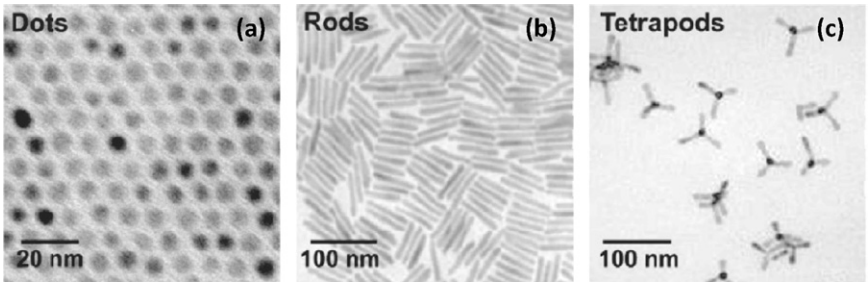

Fig. 1. TEM images of CdSe nanoparticles of differing geometry, (a) quantum dots, (b) nanorods, and (c) tetrapods. The scale bars indicate differing physical dimensions [27].

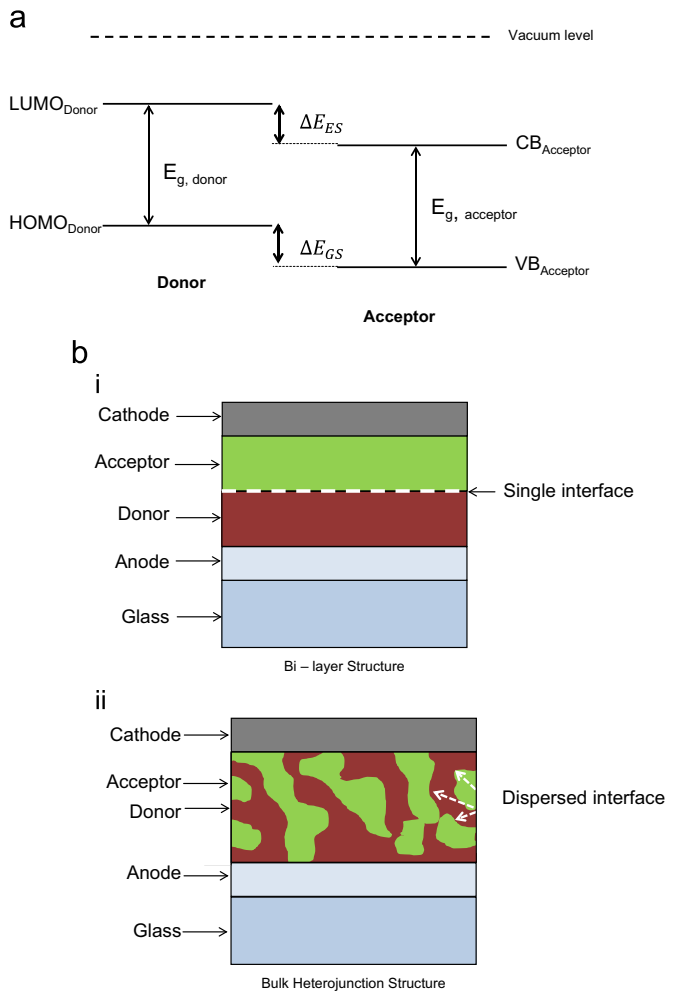

Fig. 2. (a) General energy band diagram of the heterojunction formed in a hybrid solar cell, (b) Schematic diagram of (i) bi layer heterojunction, and (ii) bulk heterojunction photoactive layers.

exciton is formed which must be dissociated by the offset in energy of the donor HOMO level and the acceptor valence band edge. The hole is then transferred to the donor at an interface and is transported to the anode whilst the electron remains in the acceptor material and travels to the cathode for collection. This process is displayed as (b) in Fig. 3. The requirements of the material electronic properties to facilitate device operation are discussed in Section 3.1.

2.3. Performance Characteristics

The power conversion efficiency (PCE) of a solar cell is defined as:

$$\mathrm{PCE} = \frac{J_{sc} \times V_{oc} \times FF}{P_{in}} \quad (1)$$

where J_{sc} is short circuit current density, V_{oc} is open circuit voltage, FF is fill factor and P_{in} is incident input power. To allow for valid comparison of device performance, an international standard for input power is used. This standard is an incident spectrum of AM 1.5 G, with an intensity of 1000 W/m^2 (100 mW/cm^2), whilst the cell is at a temperature of 25 °C. Therefore, there are three major device characteristics which completely determine the efficiency of the device. Fig. 4 displays a typical illuminated J–V characteristic curve which illustrates these three characteristics. The following describes the factors which influence these device characteristics for organic–inorganic hybrid solar cells.

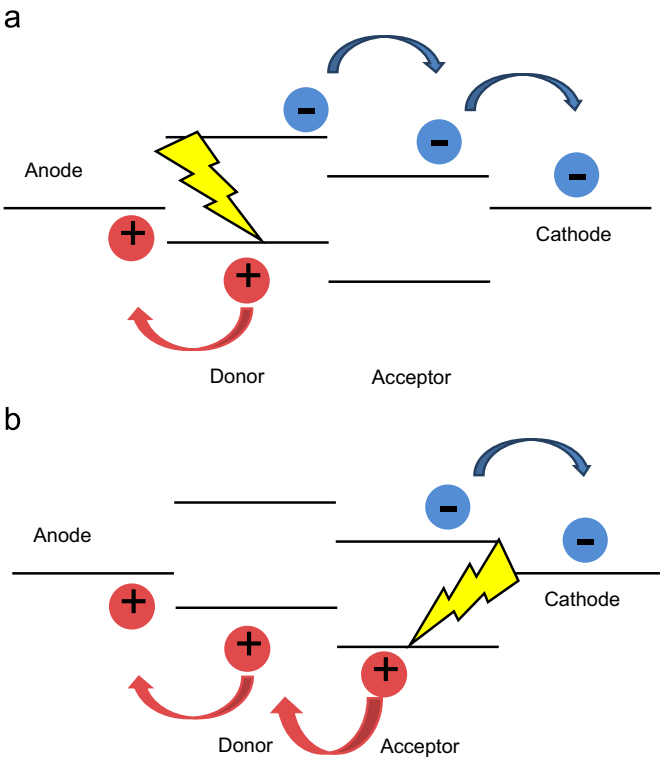

Fig. 3. Schematic diagram displaying charge transfer for (a) photo generation in the electron donor, and (b) photo generation in the electron acceptor.

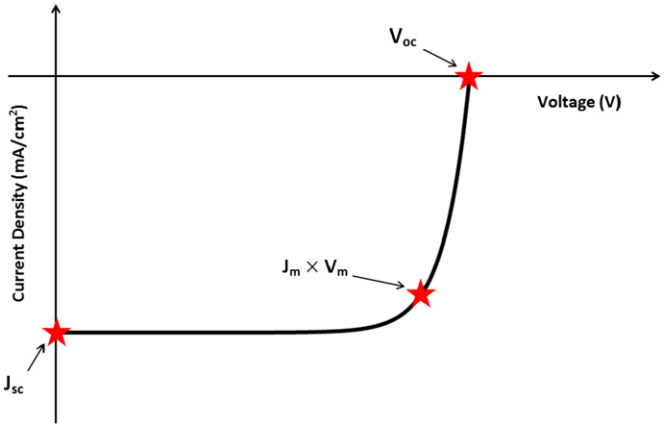

Fig. 4. Current density–voltage (J–V) characteristics for a generic illuminated solar cell. This indicates the three major device characteristics which determine PCE.

2.3.1. Short circuit current density

The short circuit current density (J_{sc}) is the maximum photocurrent density which can be extracted from the device at short circuit conditions. The J_{sc} is directly related to the external quantum efficiency (EQE). This relationship can be expressed as:

$$J_{sc} = \frac{q}{\hbar c} \int_{\lambda_{\min}}^{\lambda_{\max}} EQE \times P_{in}(\lambda)\lambda \times d\lambda \quad (2)$$

The EQE is the ratio of photogenerated electrons collected to the number of incident photons at a specific wavelength. For the operation of a hybrid solar cell, this quantity is dependent on five major steps, each of which has some associated efficiency. Thus, EQE can be expressed as:

$$EQE = \eta_{\mathrm{abs}} \times \eta_{\mathrm{diff}} \times \eta_{\mathrm{diss}} \times \eta_{tr} \times \eta_{cc} \quad (3)$$

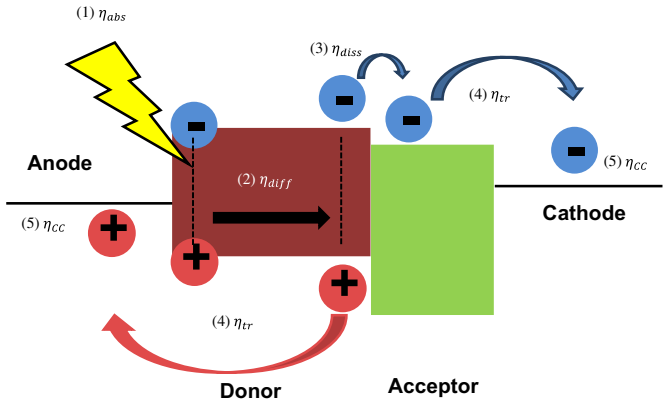

Fig. 5. Energy band diagram illustrating the five key steps in the charge transfer process. The efficiency of these steps determines the *EQE* of the hybrid device.

The parameter η_{abs} describes the absorption yield of the device, which is displayed as (1) in Fig. 5. This represents the most effective way of increasing the J_{sc} of a hybrid device [35]. The absorption spectrum of the material is determined by both the band gap and absorption coefficient of the material, whilst the thickness of the active layer will also affect the absorption yield [36]. Additionally, thin film interference will affect the absorbance of the bulk heterojunction photoactive layer. Current investigations using low band gap polymers are aimed at improving this characteristic [37–39]. In hybrid solar cells, significant useful absorption may be provided by the inorganic acceptor material. This implies that the electronic composition of the inorganic material will impact the J_{sc} of the device.

The parameter η_{diff} (Fig. 5(2)), describes the ability of an exciton to diffuse to a D–A interface. This is dependent on both the excitonic diffusion length, which is a material property, and the distance between excitation and the nearest interface, which is related to the nanoscale design of the photoactive layer. As the excitonic diffusion length in conjugated polymers is very low [31–33], control over the D–A arrangement is crucial for successful exciton diffusion. This factor is inversely related to the rate of recombination within the photoactive material.

The parameter η_{diss} (Fig. 5(3)), is the exciton dissociation yield. As the electron is still bound within the exciton, the energy offset formed at the D–A interfaces is required to provide a driving force which releases the electron and allows conduction to occur. This energy offset must be larger than the excitonic binding energy in the material to facilitate charge transfer. This energy is typically in the range of 0.1–0.5 eV [31,40]. This occurs only at the boundaries between the two materials and therefore, the distribution of the interface throughout the active layer is vitally important for the efficiency of the solar cell.

The parameter η_{tr} (Fig. 5(4)), describes the efficiency of charge carrier transport throughout the device. In organic materials, charge transport occurs via a process of hopping between energy states and is affected by traps and recombination sites in the photoactive film. The success of this transport depends greatly on the mobility of the associated semiconductors [41].

The parameter η_{cc} describes the efficiency of charge collection at the electrodes. This represents the ability of the charge carriers to be injected into the electrodes from the photoactive layer. The success of this step is greatly dependent on the electronic composition of the device. For successful injection of electrons into the cathode, the magnitude of the conduction band edge energy level of the acceptor material, with respect to the vacuum level, must be lower than the work function of the metal. For successful injection of holes into the anode, the magnitude of the HOMO level of donor material must be higher than the work function of the transparent anode. This is displayed schematically in Fig. 3. The material used for the electrodes must be carefully selected. A discrepancy between the work function of the anode and cathode material is required to provide a direction for the photocurrent. Often intermediate layers between the photoactive layer and electrodes are introduced to make the injection of charge carriers more energetically favourable [42,43]. The quality of the ohmic contact with the cathode, which is determined by the nature of the interface with the aluminium, also influences the charge collection efficiency.

2.3.2. Fill factor

The fill factor describes the 'squareness' of the *J–V* curve. It is defined as:

$$\text{Fill Factor} = \frac{J_m \times V_m}{J_{sc} \times V_{oc}} \tag{4}$$

where J_m and V_m are the maximum power point current density and voltage, respectively. This ratio is illustrated in Fig. 4. Due to physical constraints on diode quality, the practical limit to fill factor is less than the ideal value of 1. The behaviour of a real diode will deviate from the ideal, primarily as a result of recombination occurring at the junction. For OPV and organic–inorganic hybrid solar cells, the 'junction' is the D–A interface, which is distributed throughout the entire photoactive layer. Deviations from the ideal case, and thus the shape of the *J–V* curve, can be quantitatively characterised by the parasitic loss mechanisms of series and shunt resistance. Zero series resistance ($R_s=0$) is ideal, however, poor conductivity through the active layer and reduced charge carrier injection to the electrodes represents increased series resistance. Conversely, the ideal diode case demands infinite shunt resistance ($R_{sh}=\infty$). Reduction in R_{sh} is caused by imperfections within the photoactive film or current leaks at the interface between layers in the device [44].

Crystalline inorganic solar cells can achieve very good diode quality. Solar cells fabricated using silicon, GaAs and InP have achieved fill factors in excess of 80% [1,45]. Bulk heterojunction solar cells generally display significantly lower fill factors. Non-ideal nanomorphology and discrepancy between electron and hole mobility are considered as primary influences. Additionally, the active layer/cathode interface can play a major role in determining fill factor [46].

A further, troubling issue for bulk heterojunction devices is the degradation of fill factor with time, as a result of a non-stable nanomorphology and incorporation of oxygen and water vapour [47,48].

As the diode quality of a bulk heterojunction device depends heavily on the nanomorphology and interfacial area of the photoactive layer, control over these components are crucial to suppress recombination and thus allow high fill factors to be achieved.

2.3.3. Open circuit voltage

In contrast to silicon *p–n* junction solar cells, the origin of open circuit voltage in bulk heterojunction devices is still not well understood. Multiple reports have investigated this property for OPV devices, using PCBM as the electron acceptor. In 2001, Brabec et al. proposed an effective band gap model for bulk heterojunction cells, whereby the maximal value of V_{oc} is related directly to the energy difference between the HOMO level of the donor and the LUMO level of the acceptor [49]. This proposition was verified by an empirical investigation of the effect of fullerene acceptor strength (electron affinity) on open circuit voltage. A linear relationship between acceptor strength and open circuit voltage was discovered. This study also showed that V_{oc} is weakly dependent on the type of metal used as the cathode.

In 2006, a breakthrough communication on the matter was published by Scharber et al. This report studied the relationship between the energy levels of the D–A blend and the open circuit

voltage for 26 different bulk heterojunction devices. For each device, the acceptor material used was kept constant (PCBM), whilst the donor material was varied. It was found that there exists a linear relationship between the HOMO position, which is related to the diagonal band gap of the heterojunction, and the open circuit voltage [50]. From this analysis, a simple relationship between the HOMO of the donor material and the V_{oc} of the device was derived. This was reported as [50]:

$$V_{oc} = \left(\frac{1}{e}\right)\left(|E^{\text{Donor}}\text{HOMO}| - |E^{\text{PCBM}}\text{LUMO}|\right) - 0.3\ \text{V} \quad (5)$$

This suggests that V_{oc} is directly proportional to the diagonal band gap of the heterojunction; however, there exists an empirical loss factor related to the bulk heterojunction design. The systematic nature of this study made the proposition of the effective band gap model convincing, however, these results are derived purely from empirical evidence, rather than theoretical understanding. Vandewal et al. discovered a similar relationship by analysing charge transfer absorption using Fourier-transform photocurrent spectroscopy. The *EQE* spectra of polymer:PCBM solar cells was analysed for photon energies which do not overlap with the absorption bands of either the polymer or PCBM. Photocurrent response at these energies is attributed to charge transfer complexes created at the polymer:PCBM interface. It was suggested that the spectral position of this charge transfer band correlates to the diagonal band gap of the heterojunction [51]. This effective band gap can be extracted from the onset of photocurrent generated by the charge transfer band. The authors thus conclude that the V_{oc} is, in fact, related to this effective band gap. They obtained the following linear fit to describe V_{oc} [51]:

$$V_{oc} \cong \frac{E_g}{q} - 0.43V \quad (6)$$

where E_g is the charge transfer complex band gap, which is considered as the effective band gap of the heterojunction.

Vandewal et al. extended this idea from a purely empirical argument, to one which incorporates the seminal work of Shockley and Queisser [52]. Detailed balance theory suggests that maximal V_{oc} will be obtained when recombination is exclusively radiative. Large luminescence quenching in bulk heterojunction blend films implies that radiative recombination is only a small fraction of total recombination, and thus, practically achieved values of V_{oc} are far removed from the optimum value [53]. The authors suggest that V_{oc} in OPV devices is thus hindered primarily by non-radiative recombination at the D–A interface. This report uses the commonly known equation for V_{oc}, which is determined by re arranging the ideal diode equation at a value of $I=0$, to calculate predicted V_{oc}. The detailed balance limit was incorporated by using the following expression for dark saturation current density, J_0 [53]:

$$J_0 = \frac{q}{EQE_{EL}} \int EQE_{PV}(E) \times \phi_{BB}(E) \times dE \quad (7)$$

where EQE_{EL} is the electroluminescent *EQE*, EQE_{PV} is the photovoltaic *EQE* and ϕ_{BB} is the black-body spectrum at 300 K. The experimental work suggests that V_{oc} is, in fact, related to the spectral position of the charge transfer band, which is determined mainly by the energetics of the HOMO level of the donor and the LUMO level of the acceptor [53]. This approach, which is grounded in theory, explains the previously observed correlation between V_{oc} and diagonal band gap.

Recorded values of EQE_{EL} were low for the bulk heterojunction devices studied, as a result of non-radiative recombination pathways. This caused poor carrier lifetimes, which increased J_0, reducing V_{oc}. To successfully improve and optimise V_{oc}, and thus efficiency, the precise mechanism causing this non-radiative recombination must be understood [53].

A recent, contradictory report found no linear relationship between the diagonal band gap of the heterojunction and V_{oc} [54]. It was shown; however, that diagonal band gap serves as an upper bound for V_{oc}. Such reports highlight the remaining ambiguity regarding the origin of V_{oc} in bulk heterojunction OPV devices.

The origin of V_{oc} in organic–inorganic hybrid solar cells remains thus far largely unexplored. Few reports have shown a link between the diagonal band gap and V_{oc}. One report investigating hybrid polymer/TiO_2 solar cells suggests that the V_{oc} is dependent on the ionisation potential, or HOMO energy level, of the polymer [55]. This presents the view that the effective band gap model is transferrable to hybrid solar cells. The authors suggest that V_{oc} may be optimised by tuning the position of the conduction band edge in the inorganic material by molecular modification. Brandenburg et al. recently showed that the V_{oc} of P3HT:CdSe hybrid solar cells depended heavily upon the size of the CdSe nanocrystals [56]. This dependence was attributed to the size-related shift of the conduction band edge of the CdSe nanocrystals. These findings are in line with the effective band gap model suggested for OPV devices, however, much uncertainty remains regarding the exact mechanisms governing this fundamental property in hybrid solar cells.

Current understanding, at the very least, suggests the maximal theoretical V_{oc} of an organic–inorganic hybrid solar cell is determined by the diagonal band gap of the heterojunction. The requirement to maximise diagonal band gap for V_{oc} is in conflict with the desire to minimise the band gap of the individual isolated materials, such that light absorption can be maximised. Understanding this trade-off is necessary for the design and optimisation of materials used in hybrid solar cells.

3. Materials

The choice of materials used in hybrid solar cells is crucial to the overall efficiency, and thus the success of this technology. This section details the ideal properties of an inorganic material used as the electron acceptor in a hybrid solar cell. It then surveys the materials which have currently been investigated, analyses the specific materials with reference to the aforementioned desired properties and also explains the advantages of each major material group. It then summarises the major limitations faced by the use of inorganic acceptor materials, and details possible methods for improvement.

3.1. Ideal design properties

3.1.1. Donor material

When choosing a donor material, it is important to consider both electronic composition properties and hole mobility. Of particular importance are the band gap and the HOMO and LUMO levels, with respect to the acceptor material. Scharber et al. suggested that efficiencies exceeding 10% may be obtainable for an all organic device (using a PCBM acceptor) if certain design rules are used when choosing the donor material. They suggest that the band gap must be less than 1.74 eV and the LUMO level less than-3.92 eV, with respect to the vacuum level [50]. This will allow for a relatively small band gap, which can utilise a large portion of the solar spectrum, whilst still maintaining a LUMO level offset large enough to facilitate excitonic dissociation.

Chemical structures for a collection of polymer materials used in OPV and hybrid devices are displayed in Fig. 6. Early work in OPV focussed on phenylene vinylene (PPV) as the donor material [32,34,57]. The relatively low PCEs of devices using this polymer, primarily caused by low hole mobility [41], led researchers to

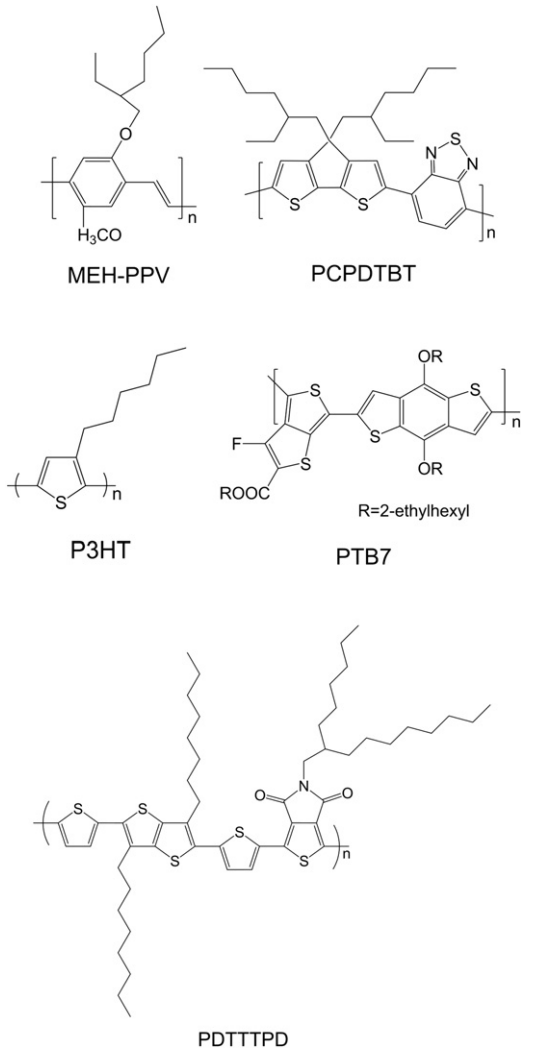

Fig. 6. Chemical structure for materials typically used as polymer donor materials. Shown are poly [2-methoxy-5-(2′-ethyl-hexyloxy)-1,4-pheny-lene vinylene] (MEH-PPV), Poly[2,6-(4,4-bis-(2-ethyl-hexyl)-4H-cyclopenta[2,1–b;3,4–b]-dithiophene)-alt-4,7-(2,1,3-benzo-thiadiazole)] (PCPDTBT), poly(3-hexylthiophene-2,5-diyl) (P3HT), Poly[[4,8-bis[(2-ethylhexyl)oxy]benzo[1,2-b:4,5-b′]dithiophene-2,6-diyl][3-fluoro-2-[(2-ethylhexyl)carbonyl]thieno[3,4-b]thiophenediyl]] (PTB7), and 2,5-di(thiophen-2-yl)thieno [3,2-b]thiophene and thieno[3,4-c]pyrrole-4,6-dione (PDTTTPD).

search for donor materials which could produce enhanced performance [58]. From about 2002 onwards, poly (3-hexylthiophene) (P3HT) became the favoured polymer donor material. Regioregular P3HT possesses many advantages when compared to PPV, such as improved absorption, improved environmental stability and higher hole mobility [59]. The all organic system of P3HT:PCBM has been exposed to intensive research, in which optimisation has occurred for parameters such as solvent used [60,61], weight % ratio of donor and acceptor [62,63], light trapping schemes [64–66] and annealing to improve the nanomorphology [67–70]. Efficiency improvements of this system however appear to have saturated, due primarily to the large band gap of P3HT, which limits the portion of the solar spectrum which can be successfully harvested.

Recently, research attention has focussed on Cyclopentadithiophene-based polymers, as they are a potential route to low band gap, high absorbing donor materials [19]. The merit of incorporating a low band gap polymer as the electron donor is illustrated in Fig. 7. It displays maximum obtainable photocurrent density (secondary axis) which is derived from AM 1.5G photon

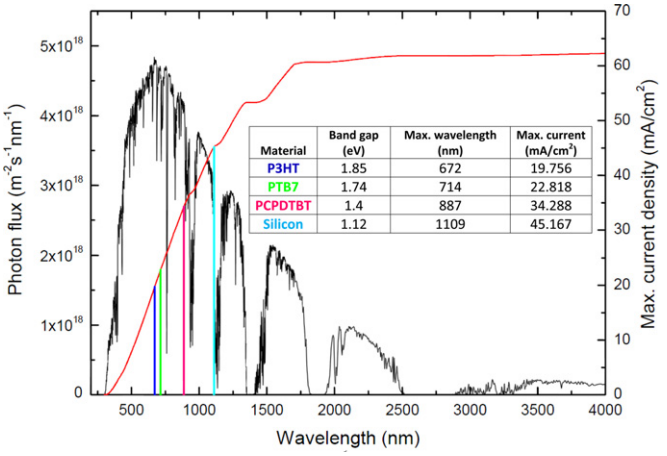

Fig. 7. Maximum obtainable values of current density (red) for multiple materials, as determined by AM 1.5G photon flux (black). This displays the effect of band gap size on determining maximum J_{sc}. The polymers P3HT, PTB7 and PCPDTBT are shown. Bulk silicon is also displayed as a reference. The inset shows a table displaying band gap, maximum wavelength of absorption and maximum obtainable photocurrent density for these materials. (For interpretation of the references to color in this figure legend, the reader is reffered to the web version of this article.)

flux (primary axis). This is calculated using the assumption that *EQE* is 100% for all wavelengths. The band gap and maximum obtainable J_{sc} for multiple polymers, as well as bulk silicon, is shown. This indicates that the potential J_{sc} for this low band gap polymer is much higher than that of P3HT.

In recent times, the polymer PTB7 has displayed excellent photovoltaic performance [71]. This polymer from the PTB family, which has a band gap of ~1.6 eV, exhibits good hole mobility, good solubility in organic solvents and polymer alignment which favours charge transport [72].

It appears as though these low band gap polymers may lead the way for future improvements in PCE for OPV and hybrid devices.

3.1.2. Acceptor material

Although fullerenes possess some desirable traits when combined with P3HT, namely excellent solubility, they also have some limitations [73]. These include limited absorption contribution and environmental stability. Replacing the fullerene with an inorganic material may help to overcome some of these downfalls. One of the main advantages of inorganic semiconductor nanoparticles is the tunability of the band gap, as a result of modifications in the physical dimensions of the nanoparticle [74].

Significant changes in band gap, with reference to the semiconductors bulk band gap, have been observed for nanoparticles used in hybrid solar cells, as a result of the quantum confinement effect [19,75,76]. A change in the band gap is related to the size of the nanoparticle, as described by the following relationship [74]:

$$E_{g,confined} = E_{g,bulk} + \frac{\pi^2 \hbar^2}{2\mu R^2} - 1.786\frac{e^2}{4\pi\varepsilon_0\varepsilon_r R^2} \quad (8)$$

where $E_{g,\mathrm{bulk}}$ is the band gap of the bulk material, μ is the reduced mass of the electron–hole pair and R is the radius of the nanoparticle. This suggests that band gaps much higher than the bulk band gap are obtainable by altering the dimensions of the nanoparticles, so that they approach the physical excitonic Bohr radius of the material.

The quantum confinement effect allows the energetic structure of the device, being both the electron affinity and ionisation potential, to be tuned, not just the optical band gap. The energetic structure of the heterojunction is crucial to the operation of a

hybrid photovoltaic device, and thus the ability to optimise this property is highly advantageous. As implied by Eq. (8), the effect of quantum confinement is particularly strong in semiconductors with low values of effective mass.

Choosing the material which may be able to do this requires close consideration to both electronic structure and additionally, physical constraints.

Xiang et al. used hybrid density functional theory to analyse the electronic structure of inorganic acceptors and also to predict the ideal qualities of a material to be coupled with P3HT, the most commonly used polymeric donor [77].

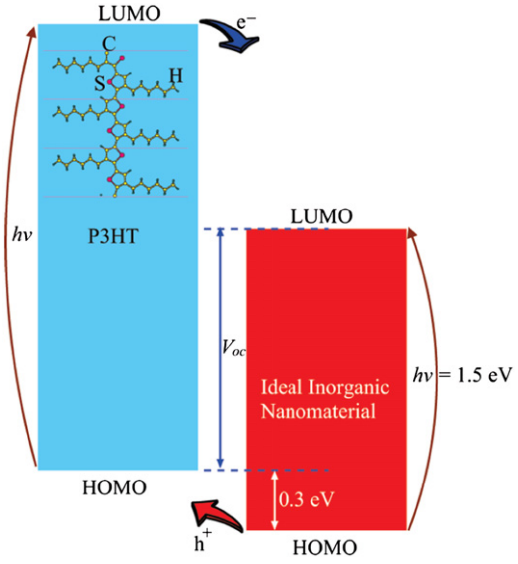

Fig. 8. Schematic illustration depicting the ideal electronic configuration for an inorganic acceptor material coupled with P3HT. The ideal inorganic nanomaterial would have both a band gap of 1.5 eV and a HOMO level offset of 0.3 eV [77].

In order to optimise the efficiency of hybrid solar cells, it is crucial to realise a trade- off based on increasing both V_{oc} and J_{sc}.

To ensure good photon absorption, and thus high J_{sc}, the band gap of the material must be minimised so that more of the solar spectrum can be utilised. Conversely, as the V_{oc} is dependent on the diagonal band gap of the heterojunction, V_{oc} will be maximised by having a high lying conduction band edge in the acceptor material. Another electronic requirement of an inorganic acceptor material is the ground state offset, with respect to the donor material. This offset level is required to facilitate excitonic dissociation when light is absorbed in the acceptor material. This component is more important in a hybrid device, as the inorganic acceptor material will contribute more useful absorption. By considering these three components, the authors have represented the ideal electronic requirements of an inorganic acceptor for hybrid solar cells in a schematic diagram. This is displayed in Fig. 8 [77].

The chosen band gap is 1.5 eV, which represents a compromise between absorption and energy offset for large V_{oc}. The HOMO level offset is chosen as 0.3 eV, which should allow for enough energy to overcome the excitonic binding energy, whilst still maximising V_{oc}. By surveying a variety of low band gap III–V semiconductors, the authors concluded that InSb quantum dots or quantum wires may possess a very desirable electronic structure for hybrid solar cells using P3HT as the donor material [77]. It is, however, important to note that this prediction is for a device which uses P3HT as the electron donor. The positions of band offsets will change when coupled with a different polymer.

Whilst this view provides a detailed analysis of the required electronic properties of a potential material, there are also many other physical considerations which may require a material compromise to be made when selecting the acceptor material. Some physical considerations include, (i) solubility in a common solvent with the donor material, (ii) abundance and cost of the inorganic material, (iii) ability to achieve a balance between electron and hole mobilities and (iv) the success of the nanomorphology of the donor/acceptor phases.

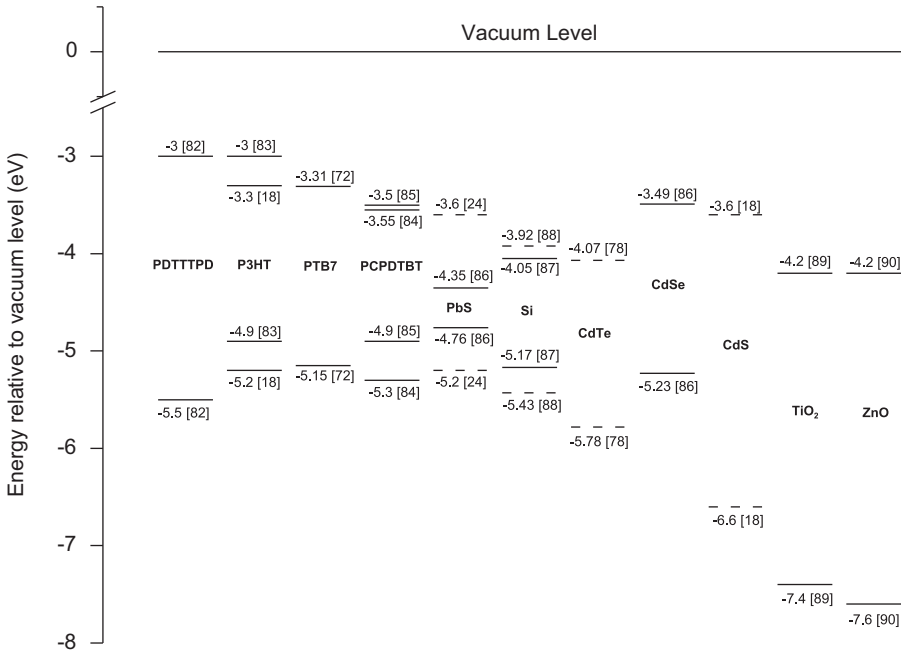

Fig. 9. Energy band diagram displaying HOMO and LUMO of possible polymer donor materials, as well as the valence and conduction band edge of multiple inorganic acceptors. Values are taken from the references displayed in the figure. For the inorganic materials, solid lines represent bulk energy values, whilst dotted lines represent nanoparticles exhibiting quantum confinement. All energy levels are measured of isolated materials, using a variety of methods. [82,18,83, 72,84–86,24,87,88,78,86,18,89,90].

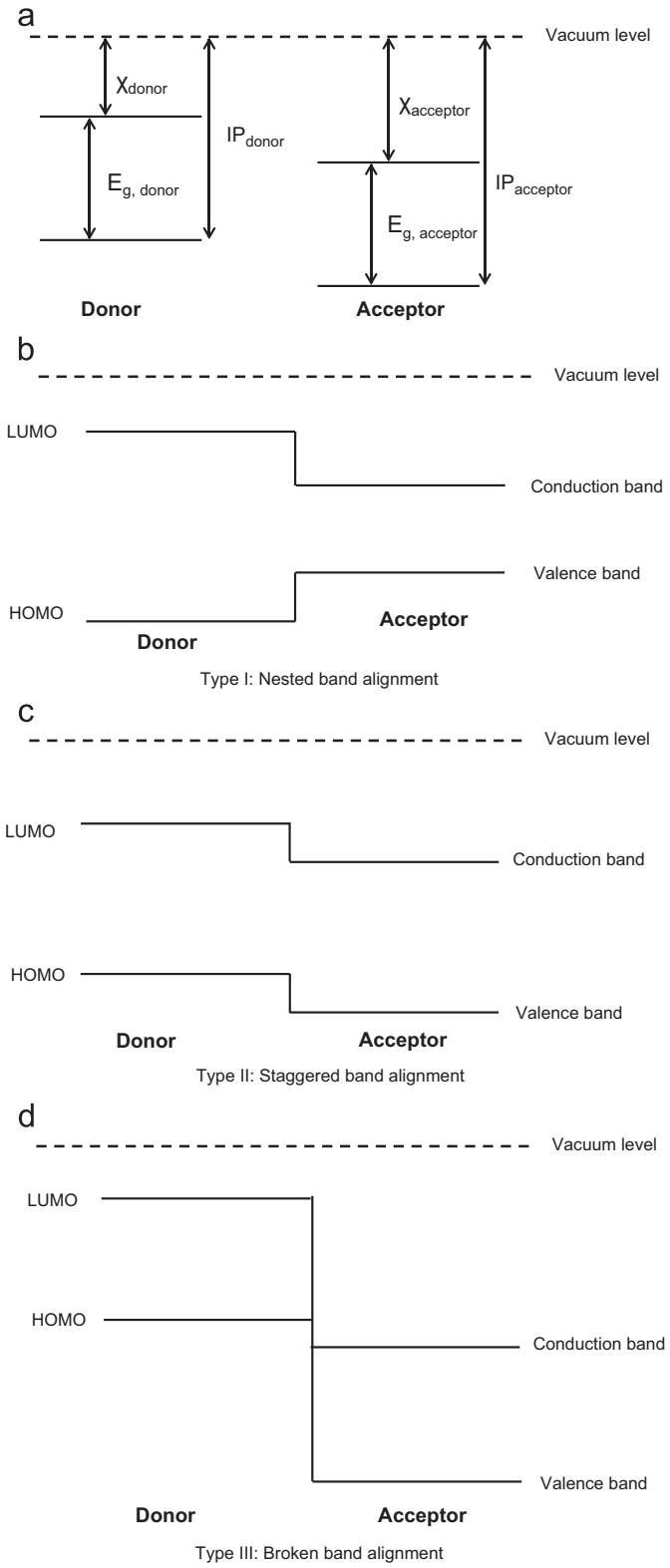

Fig. 10. (a) Energy structure of isolated donor and acceptor materials, showing band gap (E_g), electron affinity (χ) and Ionisation Potential (IP). The following shows the three major types of heterojunction structures (b) Type I: Nested band alignment, (c) Type II: Staggered band alignment and (d) Type III: Broken band alignment.

The following section details the performance of inorganic materials which have been studied thus far as acceptor materials, and aims at comparing each material group with this suggested ideal electronic structure.

3.2. Materials currently used

To date, many materials have been investigated as an electron acceptor in hybrid solar cells. These materials include CdSe [20], CdS [18], CdTe [78], Si [75], PbS [24], TiO_2 [79], ZnO [80], ZnS [81]. These materials all have unique electronic characteristics. Fig. 9 displays an energy band diagram which details the electronic structure of many materials used as an inorganic acceptor. Also shown are commonly used polymer donor materials.

When an interface is formed between two dissimilar semiconductors, an electronic heterojunction is created. The nature of this heterojunction is classified by the three material properties of (i) band gap (E_g), (ii) electron affinity (χ), and (iii) Ionisation potential (IP). Depending on these properties of the associated materials, there are three types of heterojunction which may be formed [91]. A summary of the possible heterojunction structures are displayed in Fig. 10.

The successful operation of a photovoltaic device requires a type II heterojunction, which has cascading energy levels. This is required to allow electrons to transport to the cathode and holes to transport to the anode. Analysis of Fig. 9 shows this electronic characteristic generally occurs for all of the inorganic acceptor materials when coupled with polymeric donors. This suggests that all materials may form an operating photovoltaic device; however, varied band gap, electron affinity and ionisation energy have a large impact on device performance. Other physical considerations, such as solubility in a common solvent, will also affect the performance of the device. Table 1 displays performance characteristics of various hybrid solar cells which show a variety of inorganic acceptor materials, as well as some variation in polymeric donor.

The following section will analyse the four major material groups listed in the table, being cadmium compounds, silicon, metal oxide nanoparticles and low band gap nanoparticles.

3.3. Four major material groups

3.3.1. Cadmium compounds

The current highest PCE demonstrated by an organic–inorganic hybrid solar cell was achieved by combining Cadmium Sulfide (CdS) quantum dots and P3HT nano wires [18]. Ren et al. combined a solvent-assisted chemical grafting and ligand exchange process when fabricating these high performing P3HT:CdS hybrid solar cells. The chemical grafting process involved dissolving the P3HT nanowires and CdS separately in different solvents. These two solutions were then mixed together. Fig. 11(a) displays TEM images of the P3HT:CdS system for both (a) without grafting and (b) using chemical grafting. The grafting process results in a hybrid film with a maximised interfacial area and improved interaction between the donor and acceptor phases [18]. This is evidenced by the TEM image in Fig. 11(a), and is supported by XPS analysis. Ligand exchange, using ethanedithiol was performed on the CdS QDs. This led to a decrease in the CdS interparticle distance facilitating improved charge carrier transport. Additionally, this device achieved a very high V_{oc} of 1.1 V, which was attributed to the high lying conduction band edge of the CdS QDs. This facile approach, which allows for control over the nanomorphology and enhanced interaction between the organic and inorganic material, is applicable as a general method to improve the efficiency of organic–inorganic hybrid solar cells.

Cadmium Selenide (CdSe) is a good candidate material for hybrid solar cells, as it has useful absorption in the visible region, appropriate energy levels when coupled with most conjugated polymers, and well established synthesis methods [19].

In OPV, the fullerene contributes a small fraction of the overall absorption and photocurrent, although, recent reports suggest

Table 1
A non-exhaustive list of selected parameters of hybrid solar cells utilising a range of polymer donors and inorganic nanomaterials.

Acceptor	Structure	Donor	J_{sc} (mA/cm^2)	V_{oc} (V)	*FF*	PCE (%)	Illumination (mW/cm^2)	Year	Ref.
CdS	Quantum dot	P3HT	10.9	1.1	0.35	4.1	100	2011	18
CdS	Nanocrystal	P3HT	4.848	0.842	0.532	2.17	100	2011	92
CdS	Nanowire	P3HT	5.26	0.6	0.54	1.73	-	2009	93
CdS	Nanorod	MEH:PPV	2.96	0.85	0.466	1.17	100	2007	94
CdS	Nanoporous	P3HT	5.34	0.518	0.38	1.06	100	2012	95
CdS	Quantum dot	P3HT	3.54	0.611	0.33	0.72	100	2010	96
CdSe	Nanorod:quantum dot	PCPDTBT	13.86	0.48	0.51	3.64	100	2012	97
CdSe	Nanoparticles	PCPDTBT	9.2	0.78	0.49	3.5	100	2012	98
CdSe	Nanorod	PCPDTBT	12.1	0.63	0.45	3.42	100	2012	20
CdSe	Tetrapod	PCPDTBT	10.1	0.678	0.51	3.19	100	2010	21
CdSe	Nanorod:quantum dot	PCPDTBT	8.6	0.63	0.56	3.1	100	2011	99
CdSe	Tetrapod	PDTTTPD	7.26	0.88	0.46	2.9	100	2011	82
CdSe	Nanorod	P3HT	8.79	0.62	0.5	2.9	92	2006	100
CdSe	Quantum dot	PCPDTBT	8.3	0.591	0.56	2.7	100	2011	19
CdSe	Nanorod	P3HT	9.7	0.553	0.494	2.65	100	2010	101
CdSe	Branched nanoparticles	APFO-3	7.23	0.95	0.38	2.6	100	2006	102
CdSe	Tetrapod	OC_1C_{10}-PPV	6.42	0.76	0.44	2.4	89.9	2005	103
CdSe	Hyperbranch	P3HT	-	0.6	-	2.18	100	2007	104
CdSe	Quantum dot	P3HT	5.8	0.623	0.56	2	100	2010	105
CdSe	Quantum dot	P3HT	5.5	0.78	0.47	2	100	2011	106
CdSe	Nanocrystal	P3HT	5.62	0.8	0.43	1.9	100	2012	107
CdSe	Nanospheres	P3HT	6.5	0.7	0.42	1.9	100	2011	108
CdSe	Quantum dot	P3HT	6.9	0.55	0.47	1.8	100	2009	109
CdSe	Nanorod	P3HT	5.7	0.7	0.4	1.7	-	2002	110
CdSe	Nanorod	P3HT	3.87	0.64	0.53	1.31	100	2011	111
CdTe	Tetrapod	PSBTBT-NH_2	7.23	0.79	0.56	3.2	100	2011	78
CdTe	Quantum dot	PPV	10.7	0.5	0.4	2.14	100	2011	112
CdTe	Nanorod	P3OT	3.12	0.714	0.477	1.06	100	2005	113
CdTe	Nanocrystals	PNV	6.14	0.44	0.32	0.86	100	2011	114
$CuInSe_2$	Quantum dot	P3HT	8.07	0.335	0.527	1.425	100	2011	115
graphene	Layers	CdSe	2.56	0.52	0.418	0.58	100	2012	116
PbS	Nanocrystals	MEH-PPV	0.13	1	0.28	0.7	5	2005	117
PbS	Quantum dot	P3HT	1	0.42	0.39	0.16	-	2011	24
PbS	Quantum dot	P3HT	0.3	0.35	0.35	0.04	100	2007	118
Si	Nanorod	Spiro-OMeTAD	30.9	0.57	0.588	10.3	100	2011	87
Si	Nanowire	PEDOT:PSS	24.24	0.532	0.651	8.4	100	2012	119
Si	Nanowire	PEDOT	19.28	0.47	0.61	5.09	100	2010	120
Si	Core-shell	P3HT	18.9	0.346	0.352	2.31	100	2011	121
Si	Nanowire	P3HT	11.61	0.425	0.39	1.93	100	2009	122
Si	Quantum dot	P3HT	3.8	0.8	0.47	1.47	100	2010	75
Si	Quantum dot	P3HT	3.3	0.75	0.46	1.15	100	2009	88
TiO_2	Porous	P3HT	4.71	0.87	0.68	2.81	100	2011	123
TiO_2	Nanorod	P3HT	4.33	0.78	0.65	2.2	100	2009	124
TiO_2	Nanorod	P3HT	2.73	0.64	0.56	0.98	100	2008	125
TiO_2	Nanotube	P3HT	1.8	0.62	0.58	0.5	100	2011	126
ZnO	Domains	P3HT	5.2	0.75	0.52	2	100	2009	80
ZnO	Nanoparticles	MDMO:PPV	2.4	0.814	0.59	1.6	71	2005	127
ZnO	Nanoparticles	MDMO:PPV	2.67	0.828	0.399	0.88	100	2011	128
ZnO	Nanoparticles	P3HbpT	2.1	0.83	0.35	0.61	100	2012	90
ZnO	Nanowire	P3HT	0.32	0.4	0.28	0.036	100	2010	129
ZnS	Nanoparticles	P3HT	0.0081	1.2	~0.25	~0.2	1.26	2009	81

this fraction may be larger than previously expected [22]. However, the addition of an inorganic material has the potential to provide enhanced, complementary absorption. CdSe nanoparticles contribute useful absorption to the hybrid film. In a recent communication, Dayal et al. report that 34% of the absorption of a PCPDTBT:CdSe system is attributed to CdSe [21]. This contribution has a positive impact on the device *EQE* profile, which confirms that the absorption contribution of the inorganic acceptor material leads to the production of photocurrent. The electronic structure of CdSe forms a type II heterojunction with most conjugated polymers, with appropriate energy level offsets, (HOMO/VB and LUMO/CB) which facilitates charge separation and transport. The band gap of bulk CdSe is approximately 1.74 eV, however, this is altered by changing the physical dimensions of the nanoparticle [130]. Zhou et al. report a band gap of ~2 eV for CdSe nanoparticles with a mean diameter of 4.7 nm [19]. This value is larger than ideal, nevertheless, it still allows for absorption up to ~650 nm. As seen in Fig. 9, the theoretical V_{oc} from this material has the potential to be quite high, due to the relatively high value of conduction band edge. Values of V_{oc} obtained from this acceptor material have thus far been promising, with a maximum reported value of 0.95 V [102].

The well-established synthesis methods of this material allow for the formation of nanoparticles with complicated shapes. Dayal et al. synthesised CdSe tetrapods dispersed in a polymer matrix. A TEM image of these CdSe tetrapods is displayed in Fig. 11(b). These tetrapods are reported to have average dimensions of 5 nm arm diameter and 30–50 nm arm lengths. These physical dimensions allow for an improved nanomorphological structure, which facilitates excitonic dissociation and leads to improved

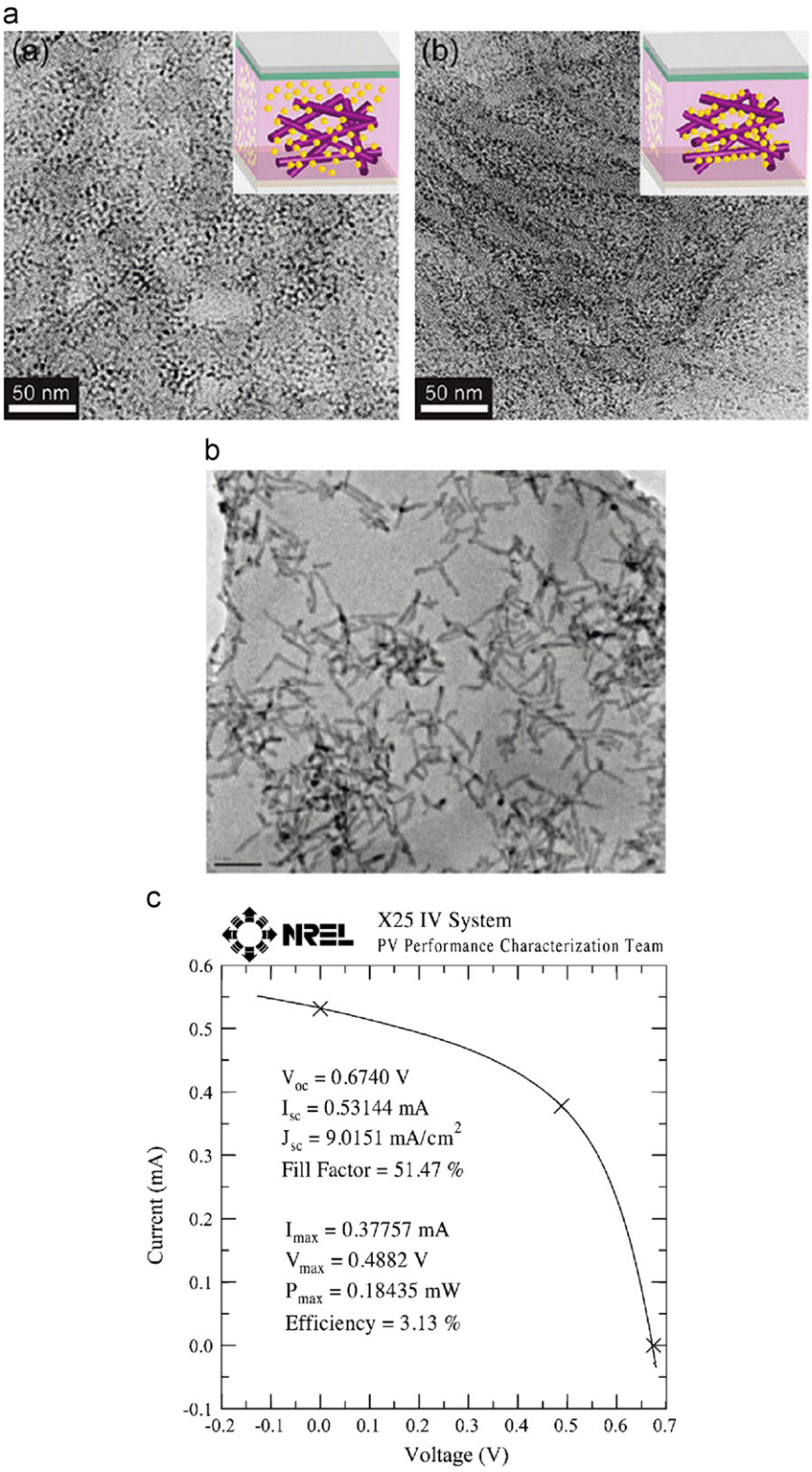

Fig. 11. (a) TEM images of the P3HT:CdS system without chemical grafting (a) and with chemical grafting (b) [18], (b) TEM image of CdSe tetrapods, with a 50 nm scale bar [21], (c) Current density–voltage characteristics for the PCPDTBT:CdSe solar cell, as certified by NREL [21].

conductive pathways [21]. As a result, the ordered structure leads to improved electrical characteristics. Fig. 11(c) shows the certified *I–V* profile of this device which uses tetrapods.

One major drawback of this material is its toxicity; however, it may be a good model system to study to gain a deeper understanding of hybrid solar cells.

3.3.2. *Silicon*

Silicon is a good candidate material for hybrid solar cells due to its abundance, non-toxicity and strong absorption in the UV region [88]. Additionally, the higher dielectric constant of silicon, compared with PCBM, prevents back transfer and improves transport away from the interface [131]. Silicon forms a strong

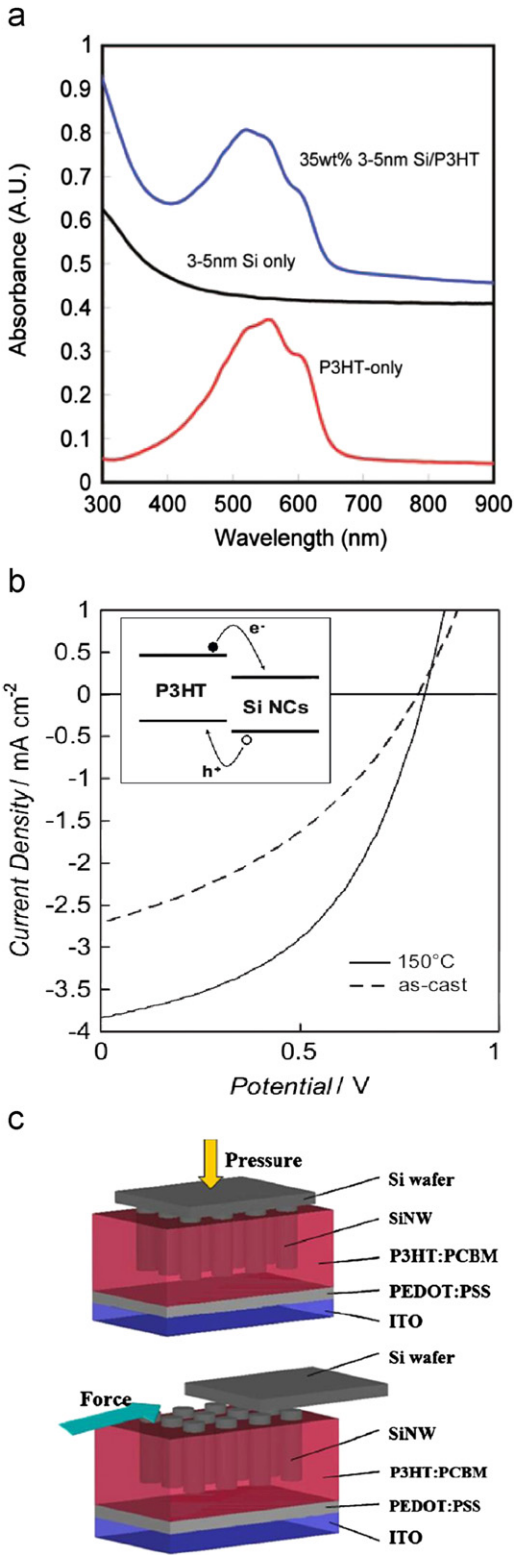

Fig. 12. (a) Optical absorption spectra for P3HT, silicon nanocrystals and P3HT:Si NC blend film [88], (b) *J–V* characteristic curves of P3HT:Si NC solar cells under 100 mW/cm^2, AM 1.5 G conditions. This shows a comparison of an as-cast and annealed device. The annealing conditions were 150 °C for 120 min [75], (c) Schematic diagram of the procedure used to form hybrid solar cells incorporating silicon nanowires. First, the nanowires were pressed into the P3HT:PCBM blend, then the wafer was removed by the application of lateral force [122].

type II heterojunction when coupled with P3HT. The band gap of bulk silicon is 1.12 eV [132]. Quantum confinement of silicon nanocrystals (Si NCs) increases the band gap [133], which makes the electronic properties of the material even more desirable. Liu et al., reported that the band gap of Si NCs, with an average size of 3–5 nm, was approximately 1.5 eV, as evidenced by a change in photoluminescence measurements when compared to bulk silicon [75]. Thus, the electronic structure of silicon nanocrystals is close to the ideal structure discussed in Section 3.1.

Due to this relatively small band gap, Si NCs are able to provide an enhanced absorption profile. This enhancement is almost exclusively in the UV region, due to the weak absorption coefficient, when compared to P3HT. An absorption profile of a P3HT:Si NCs blend is displayed in Fig. 12(a). This favourable electronic structure also allows for a relatively high value of V_{oc} to be achieved, as the conduction band edge is shifted up due to quantum confinement. Open circuit voltage values of up to 0.8 V have been recorded, which exceeds that of the P3HT:PCBM blend [75]. Liu et al. showed that tuning the size of Si NCs led to a change in band structure which, in turn, led to a change in performance. It was shown that NCs with small physical dimensions, 3–5 nm, provided the best PCEs due to both an improved V_{oc} and I_{sc} [88].

In a recent publication, the same authors produced a device with an improved PCE of 1.47%. This was achieved by optimisation of an annealing step. The annealing parameters found to be optimum, which were 150 °C for 120 min, are different to those established for P3HT:PCBM blends. The current–voltage characteristic curve, displaying PCE improvement due to thermal annealing, is shown in Fig. 12(b). An increase of both I_{sc} and fill factor is achieved as a result of annealing. This is attributed to an increase in hole mobility, which leads to a more balanced device mobility. This causes a reduction in the build-up of space charge and a reduction in recombination [75].

The PCE of these hybrid devices is still very low. This is attributed mainly to non-uniform nanomorphology, due to the agglomeration of silicon nanoparticles.

An alternative to Si NCs is silicon nanowires (Si NWs). The main advantage of this approach is that the structured nature of the nanowires can help facilitate efficient charge transport.

Huang et al. have demonstrated the formation of a silicon nanowire array using a wet etching method. This method is aimed at overcoming some of the problems associated with other fabrication techniques, such as chemical vapour decomposition (CVD) and laser ablation [122]. Si NWs, formed on a silicon wafer, were incorporated into a P3HT:PCBM blend film by heating the film to 160 °C and applying a downwards pressure. A lateral force was then used to separate the silicon wafer from the P3HT:PCBM film. This process is displayed in Fig. 12(c).

Characterisation of this hybrid device revealed that the Si NWs contributed to absorption in both the near infra-red and visible regions. The spectral window of this device was widened, with respect to the control P3HT:PCBM device, due to the smaller band gap of Si. The increased charge carrier mobility of the Si NWs is an additional advantage.

Current–voltage characteristics revealed a significant increase in J_{sc} due to the addition of the Si NWs. The value increased from 7.17 mA/cm^2 to 11.61 mA/cm^2, which was attributed to both improved charge transport and enhanced absorption spectra.

These initial results show promise for the viability of silicon in hybrid solar cells, particularly due to its elemental abundance and non-toxicity.

3.3.3. Metal oxide nanoparticles

Wide band gap oxide semiconductors have also been explored as inorganic acceptors in hybrid solar cells. Materials which have been investigated include TiO_2, SnO_2, CeO_2, and ZnO [26,134,135].

The major advantage possessed by these semiconductors is the ability to form vertically aligned oxide nanostructures. Such

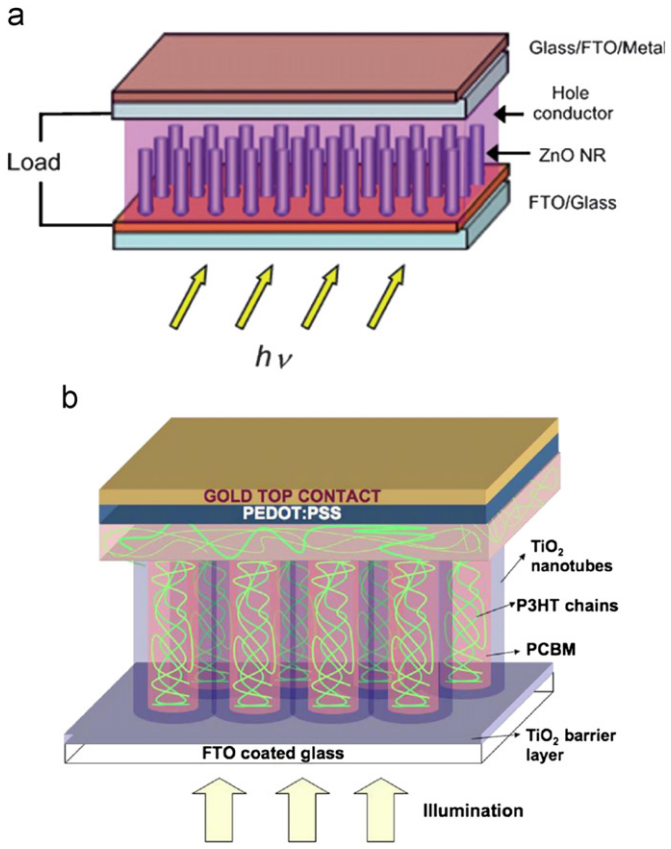

Fig. 13. (a) Schematic diagram of a hybrid solar cell applying a vertically aligned structure of ZnO nanorods as the electron acceptor. The hole conductor is a conjugated polymer matrix [26], (b) Schematic diagram illustrating the double heterojunction formed between TiO_2 nanotubes and P3HT:PCBM [142].

ordered structures may be engineered so that the physical dimensions allow for optimisation of a large D–A interfacial area, as well as providing efficient conduction pathways [136]. This allows for a large dissociation yield, as well as reduced electron hopping steps, thus increasing electron mobility. A schematic diagram of such a structure is shown in Fig. 13(a) [26]. Currently, the most heavily investigated of these materials is TiO_2, as it has been extensively used in dye sensitised solar cells due to the high surface area of the semiconductor [137–141].

The electronic structure of TiO_2 is not, however, desirable for use as an inorganic acceptor material. This is shown in Fig. 9. The wide band gap, which is characteristic of oxide compounds, leads to negligible absorption contribution in the visible spectrum. Although the band gap is large, the position of the conduction band edge, which forms a type II heterojunction with the appropriate polymeric materials, yields a maximum obtainable V_{oc} which is similar to that of PCBM. Reported values of V_{oc} for hybrid solar cells using oxide compounds tend not to be very high.

Mor et al. have demonstrated this principle for TiO_2 nanotubes infiltrated with a P3HT:PCBM blend [142]. A schematic diagram of the created structure is shown in Fig. 13(b). This structure forms a double heterojunction, as charge can be separated at both the P3HT:PCBM and P3HT:TiO_2 interface. The good device performance is attributed to efficient charge generation and ordered device geometry.

A current, promising communication has exhibited the fabrication of anatase phase vertical TiO_2 nanowires, using an electrospinning process. Anatase phase TiO_2, rather than rutile phase TiO_2, is preferred for optoelectronic applications, due to its better electron transport and reduced charge carrier recombination [79]. The authors suggest that current synthetic methods may be inadequate for growing highly ordered nanowires, due to the limited ability to tune the important characteristics of nanowire diameter, height and packing density. Optimisation of this electrospinning method, to produce high throughput anatase nanowires, with appropriate physical dimensions for photovoltaic purposes, may lead to a significant enhancement in this field.

Recently, research interest has focussed on ZnO as an appropriate material. This is because it has a very similar electronic structure to that of TiO_2, however, it has some advantages in comparison. First, it tends to have higher electron mobility than TiO_2. Additionally, it can be synthesised using a variety of techniques. This makes it attractive for low cost scalable solar cell fabrication [26,135].

Although it has many available synthesis methods, it is very difficult to determine which is most suitable for photovoltaic applications, as the PCE of the photovoltaic device depends on multiple parameters besides the ordered structure of the active layer.

The hydrothermal growth method is seemingly the most attractive approach to forming well-aligned nanostructures. Although ZnO has great potential, current synthesis methodologies have been lacking, due to limited reproducibility and the inability to form structures with the required physical dimensions to optimise photovoltaic performance. Due to the short excitonic diffusion length for polymeric donors [31–33], a dense array of vertically aligned crystals is desired; however, the physical replication of such a system, leading to devices with high PCEs, has not yet been produced.

Asides from forming the physical structure, both wettability and stability are problems for ZnO. Wettability is the infiltration of the hole conducting polymer into the oxide network. For good photovoltaic performance, the polymer must penetrate the entire surface of the oxide, which is difficult to achieve for a densely packed structure with a very large surface area. Another problem which arises from the polymer infiltration is that the arrangement of the material is inferior to that of the polymer chain packing in a bulk active layer, due to the more random orientation. This causes lower hole mobility than for polymers in a flat BHJ device [142].

An understanding of the polymer phase orientation within the oxide nanoarray is crucial in improving the performance of these devices, such that the potential improvements associated with highly ordered bulk heterojunctions can be realised. The physical properties and orientation of regio-regular P3HT, confined within a TiO_2 nanoarray, was investigated by Foong et al. [143]. They suggested that gravity and capillary forces alone are insufficient to produce complete infiltration of P3HT into the dense nanoarrays. To achieve infiltration, the system was annealed at 250 °C under a vacuum of 20 mTorr. Cross sectional SEM images indicated that complete polymer infiltration was successfully achieved using this method. XRD analysis of non-confined and nano-confined P3HT indicated that edge-on orientation was present for both cases; however, the intensity of the peak for nano-confined P3HT was significantly reduced. This suggests a higher degree of crystallinity for the non-confined P3HT, and a more random arrangement for the nano-confined P3HT. *EQE* measurements of P3HT:TiO_2 nanotube hybrid devices showed that devices using vertically aligned nanostructures led to improved device performance, with reference to the bilayer benchmark device, however, the improvement was only weakly correlated with the improvement in interfacial area. It was suggested that the orientation of the polymer, which determines the hole mobility of the system, influences the success of charge transport throughout the device. As measured by XRD, the orientation of P3HT in the nano-confined systems was edge-on. This polymer orientation is undesirable for charge transport and was the reason assigned to the small improvement. Perhaps the key to unleashing the potential of well aligned bulk heterojunction structures is substituting P3HT with a different polymer, which can achieve better orientation and hole mobility when nano-confined.

The stability of hybrid solar cells using ZnO has also been questioned [26]. The mechanism of oxygen release from the oxide material is detrimental to the polymer material. This can lead to a rapid reduction in reported device performance. It has also been observed that irradiation with UV light can also drastically reduce the device output.

Shao et al. have suggested a method of enhancing the stability of a MEH–PPV:ZnO device by introducing an optical layer to decrease UV light in the active layer [144]. This was achieved by depositing a ZnO layer of varying thicknesses between the active layer and aluminium cathode. This appeared to result in an improvement in the stability of the device under illumination.

3.3.4. Low band gap nanoparticles

One of the main purposes of inherently low band gap materials is to extend the spectral window of solar cells, to that of longer wavelengths [35,145,146]. Generation of photocurrent in the NIR range is particularly useful as it will reduce the heating effect attributed to these wavelengths, as well as increasing the J_{sc}. This potential trait of low band gap inorganic nanoparticles is particularly useful when coupled with polymers which have absorption limited to the visible region, such as P3HT [24].

Pb-based nanoparticles are popular for investigation due to their ability to absorb in the near infra-red (NIR) region. The band gap of bulk PbS, 0.41 eV, is quite low [147]. The position of the valence band of PbS does not facilitate efficient hole transport to the polymer, which means that excitons formed in the QD cannot become successfully dissociated. The band structure formed is thus a weak type II heterojunction. Additionally, the size of the band gap implies that the maximum obtainable V_{oc} value is quite low.

Guchhait et al. included TiO_2 nanorods with P3HT:PbS solar cells. TiO_2 is a very strong electron accepting agent due to the position of its valence band edge. A drastic increase in short circuit current was observed for devices with TiO_2 [24]. Without the TiO_2 nanorods, absorption in the NIR cannot be converted to photocurrent due to the energetically unfavourable conditions, however, the addition of TiO_2 lead to these excitons becoming dissociated and thus contributing to the device performance. The *I–V* curves of devices (a) without a TiO_2 layer and (b) with TiO_2, are displayed in Fig. 14(a).

The authors also demonstrate the ability to tune the electronic structure by changing the physical dimensions of the QD. By varying the diameter of the nanoparticle, differences in photocurrent are observed. By illuminating the devices through an infra-red filter, a photovoltaic response is recorded. The *I–V* curves, for devices fabricated with varying physical dimensions, are shown in Fig. 14(b).

An apparent optimum QD diameter is established. This is attributed to two factors: (i) the reduction in absorption for smaller QD diameters and (ii) the level of the conduction band relative to the conduction band edge of TiO_2.

It is generally difficult to achieve a type II heterojunction using low band gap inorganic electron acceptor. Even if this is achieved,

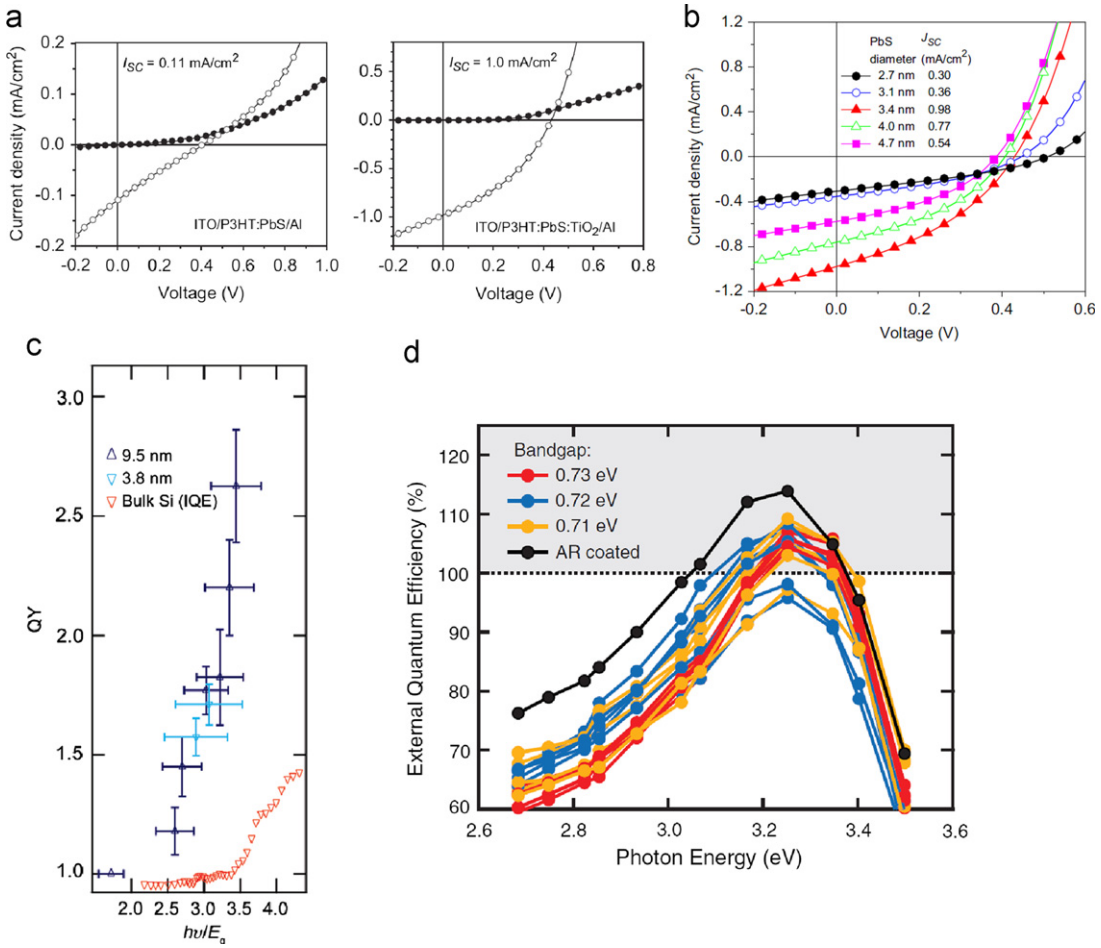

Fig. 14. (a) Dark (filled circle) and illuminated (open circle) *J–V* characteristics for P3HT:PbS hybrid solar cells without (left) and with (right) TiO_2 incorporated into the active layer [24], (b) Light *J–V* characteristic curves for P3HT:PbS:TiO_2 devices, displaying varying size PbS quantum dots [24], (c) MEG quantum yields for silicon nanocrystals samples of size 9.5 nm (dark-blue triangles) and 3.8 nm (light-blue triangles), plotted as function of the ratio of photon energy divided by band gap. The red triangles display impact ionisation yields for bulk silicon [150], d) *EQE* peaks for PbSe QD solar cells. Devices were fabricated with varying QD band gap, as well as a device with an anti-reflection coating [151]. (For interpretation of the references to color in this figure legend, the reader is reffered to the web version of this article.)

it will be difficult to achieve a high PCE as absorption in the acceptor will lead to significant thermalisation losses for photons in the visible region. The phenomenon of "Multiple Exciton Generation" (MEG) presents a promising route for efficiency enhancements in hybrid solar cells using low bad gap inorganic acceptor nanoparticles [148].

MEG is the process in which multiple electron–hole pairs can be generated by single, high energy photons. In bulk semiconductors, this process is very inefficient as the threshold photon energy for MEG is very high, due to the requirement of crystal momentum conservation. Additionally, the rate of generation must compete with the rate of relaxation via electron–phonon scattering [149]. As a result, the photon energies required for MEG are not generally useful for solar energy conversion. In nanoparticles, the effectiveness of MEG is greatly enhanced, due to the relaxation of the requirement for conservation of momentum. The lower threshold required for MEG means that this phenomenon may be observed at photon energies useful for solar energy conversion.

Beard et al. examined MEG in silicon nanocrystals using transient absorption spectroscopy. They found the threshold energy for MEG, for 9.5 nm diameter silicon nanocrystals, to be 2.4 ± 0.1 E_g [150]. A plot of quantum yield as a function of photon energy, divided by band gap energy, is displayed in Fig. 14(c). A quantum yield of 2.6 is recorded at a photon energy of 3.4 E_g. Practical application of this phenomenon can lead to photocurrent quantum yields of $>100\%$. Semonin et al. reported photocurrent enhancements in lead selenide (PbSe) quantum dot (QD) solar cells [151]. These enhancements, evidenced by *EQE* measurements, were attributed to the phenomena of MEG. Peak *EQE* values of 114% were achieved for PbSe QD solar cells, which provides conclusive proof that MEG occurs in QDs, and that this phenomenon can lead to *EQE* values higher than 100% [151]. *EQE* peaks for various PbSe solar cells are displayed in Fig. 14(d). This report holds great promise for efficiency enhancements in hybrid solar cells utilising low band gap nanoparticles.

3.4. Limitations to performance

As previously discussed, the use of inorganic acceptor materials should yield multiple advantages, such as enhanced absorption, improved conductivity and device architecture. So why is it that the current state of the art PCE values for hybrid solar cells are so much lower than that of OPV? Problems associated primarily with increased density of trap states, related to the nanoparticle surface chemistry, and limited control over the D–A nanomorphology have thus far hindered the progress of this technology.

3.4.1. Nanoparticle surface chemistry

Although inorganic semiconductors have intrinsically better conductivity, the electron mobility of inorganic materials within a polymer matrix is often very low [74]. During the synthesis process, an organic ligand material is bonded to the surface of the inorganic nanoparticle, which controls both the size and shape of the material, as well as inducing particle stability [152]. This organic ligand attached to the surface is electrically insulating, which impedes both the charge transfer at the D–A interface and reduces the mobility of electrons travelling through the acceptor phase. Increased recombination leads to significant reductions in collected photocurrent, which limits device efficiency. Attempts to increase the efficiency of hybrid solar cells have often focussed on overcoming the effect of this insulating layer, to restore the good charge carrier characteristics of the inorganic material [105,106,153]. A common method is a ligand exchange with pyridine, whereby the thick organic insulating ligand layer, introduced during synthesis, is replaced by the shorter, more conductive pyridine molecules [154,155]. This is thought to facilitate better charge transfer and transport, leading to improved

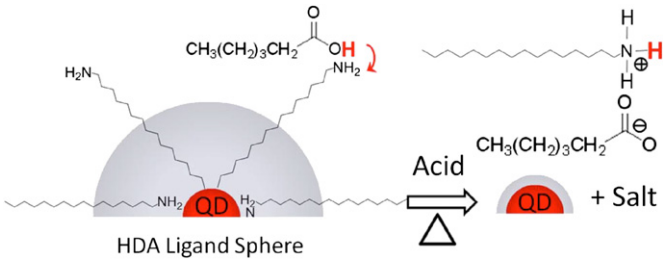

Fig. 15. Schematic diagram illustrating the effect of a hexanoic acid treatment on the surface of CdSe nanocrystals. The acid removes the insulating sphere, producing a salt as a by-product, which is then easily washed away from the surface [105].

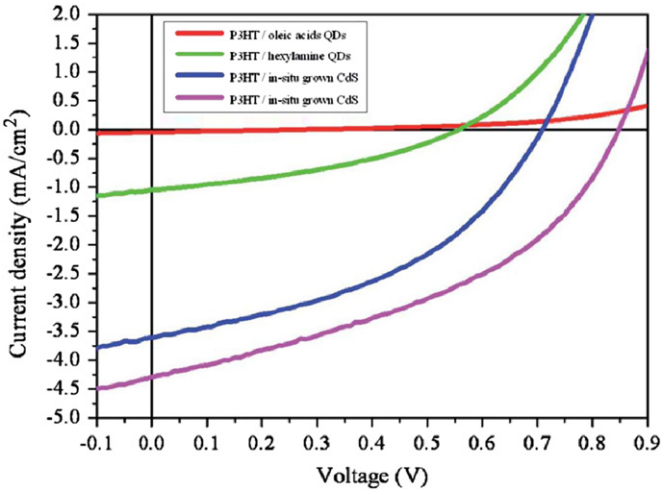

Fig. 16. Comparison of current–voltage characteristic curves of hybrid solar cells of P3HT and oleic acid-capped CdS (red), hexylamine-capped CdS (green), *in situ* grown CdS (blue) and *in situ* grown CdS with a higher CdS loading (magenta) [156]. (For interpretation of the references to color in this figure legend, the reader is reffered to the web version of this article.)

efficiencies. Dayal et al. used a pyridine treatment on the CdSe tetrapods used in their PCPDTBT:CdSe system [21]. After synthesis, the CdSe tetrapods were washed in a toluene/ethanol solution to remove some of the capping ligand. The remaining ligand was then exchanged with pyridine by heating the pyridine solution to 107 °C. The particles were then recovered by a precipitation process with hexane. This process appears to have facilitated improved charge transport in the CdSe tetrapods, thus enabling improved device PCE. It is, however, often difficult to obtain a stable polymer/NC mixture in a solvent after the NCs have undergone a ligand exchange, and thus, it is necessary to use a mixture of solvents. For the aforementioned PCPDTBT:CdSe system, a solvent mixture of chloroform/pyridine/trichlorobenzene was used. The pyridine exchange may not be complete and thus some of the initial ligand will remain after the treatment. Additionally, the exchange process may induce further undesirable trap sites by exposing dangling bonds in the nanocrystal, leading to enhanced recombination sites. It appears as though some surface modification is required; however, ligand exchange may not be the best method.

Zhou et al. recently proposed a novel approach to reduce the impact of the insulating ligand. CdSe nanoparticles were treated with a hexanoic acid washing procedure which replaced a ligand exchange procedure [105]. It is believed that this process removes the organic ligand of hexadecylamine (HDA) from the surface of the nanoparticles by the formation of a salt, when reacted with hexanoic acid. This salt can then be separated and removed more easily than the immobilised HDA ligand on the particle

surface. A schematic diagram of this process is shown in Fig. 15. This procedure led to a reduction in the size of the nanoparticle, as well as reduction in the inter-particle distance. This is thought to be the reason for improved charge transport and thus device efficiency.

This quick, simple process can be transferred to ordered nanoparticle structures, such as nanorods. The same authors have since demonstrated this concept, whereby the surface of CdSe nanorods were treated with this hexanoic acid washing procedure. Large sized nanoparticles, treated with hexanoic acid, were combined with PCPDTBT to achieve device PCEs above 3% [99]. This good performance was attributed primarily to improved charge transport throughout the inorganic network.

An alternative to ligand passivation methods is the *in situ* growth of inorganic films within a polymer [92]. Reynolds et al. demonstrated hybrid devices consisting of *in situ* grown CdS, within pre-coated P3HT films. This report displays a comprehensive comparison of hybrid systems which combine P3HT with both (i) *in situ* grown CdS films or (ii) CdS QDs synthesised with various capping ligands [156]. TEM images of both systems suggested that the *in situ* grown CdS provide an interconnected network of nanoparticles, which is conducive to improved charge transport. Transient absorption spectroscopy was used to investigate charge generation. *In situ* grown CdS blends display significantly higher polaron yield and lifetimes, when compared to oleic acid and hexyl amine capped QD blends. Additionally, increasing the loading of CdS in the *in situ* grown blend leads to longer lived generated charges. Improved charge generation was verified by current–voltage measurements. Fig. 16 displays *I–V* curves measured for both *in situ* and ligand capped CdS QDs. Due to a significant increase in J_{sc}, and a concomitant increase in V_{oc}, the device efficiency of *in situ* grown CdS blends was vastly enhanced. This was attributed to an increase in charge generation and charge collection at the electrode, due to improved nanomorphological arrangement, and reduced charge carrier recombination. The analysis suggests that the ability to generate long-lived charges is dependent on nanomorphological constraints.

3.4.2. Nanomorpholgy

The nanomorphological arrangement of donor and acceptor atoms within the active layer is important in determining device PCE [157,158], as it controls the excitonic dissociation efficiency [34]. This is crucial because of the relatively short excitonic diffusion length [31–33] and low charge carrier mobility of organic materials [159,160]. In a bulk heterojunction design, there exists a trade-off between excitonic dissociation, related to the D–A interfacial area, and the charge carrier conductivity and collection, related to the formation of percolated pathways. It appears as though the morphology of hybrid solar cells is generally more difficult to control than that of OPV devices [74]. This could be due to the agglomeration of inorganic nanoparticles into large aggregates and the requirement of a more complex solvent. As the nanocrystals and polymers have different solubilites, the solvent used for hybrid solar cells is very important. Wang et al. investigated the use of both pyridine and chlorobenzene as a solvent for a MEH-PPV:CdS mixture [94]. Characterisation using TEM shows different distributions of CdS nanoparticles in PPV as a result of different solvents. This is displayed in Fig. 17.

The film cast with pyridine solvent (image (a)) displays a much more homogenous distribution of CdS nanoparticles, with less aggregation. This is directly linked to an increased J_{sc} and photoresponsivity.

This indicates that the solvent used has a profound impact on the arrangement of the nanocrystals within the polymer. As with Dayal et al., the solvent used is generally not a single solvent, but rather a complicated mixture to allow for the differing solubilities of the donor and acceptor materials. The choice of solvent is more crucial for hybrid solar cells, and much optimisation is required for emerging material combinations.

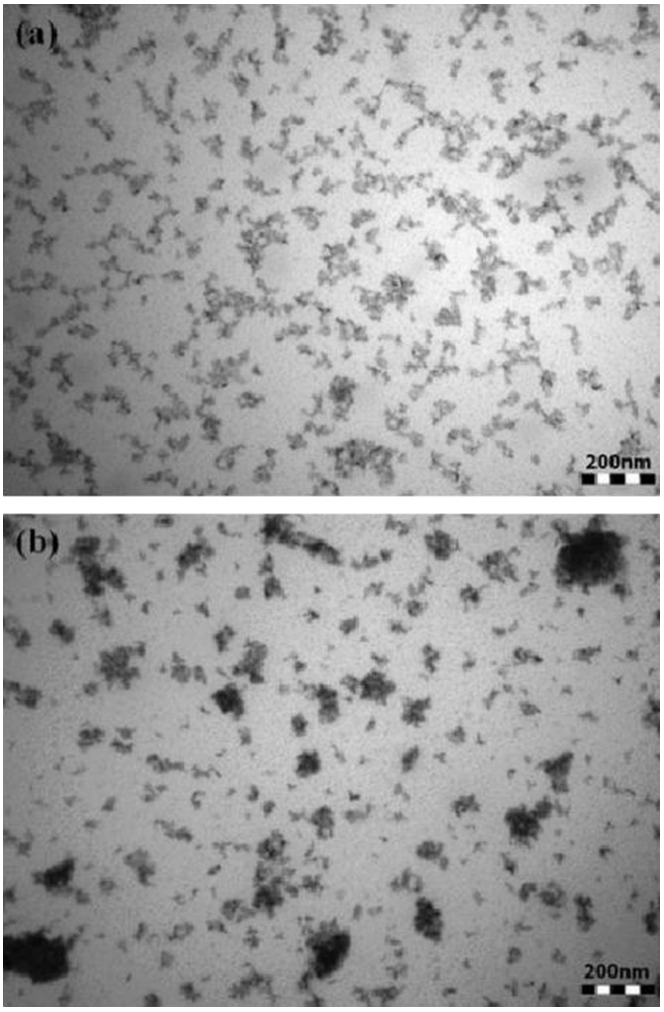

Fig. 17. TEM image of MEH-PPV:CdS film. The film contains 86 weight percentage multiarmed CdS nanorods. The films were cast using solvents of (a) pyridine and (b) chlorobenzene [94].

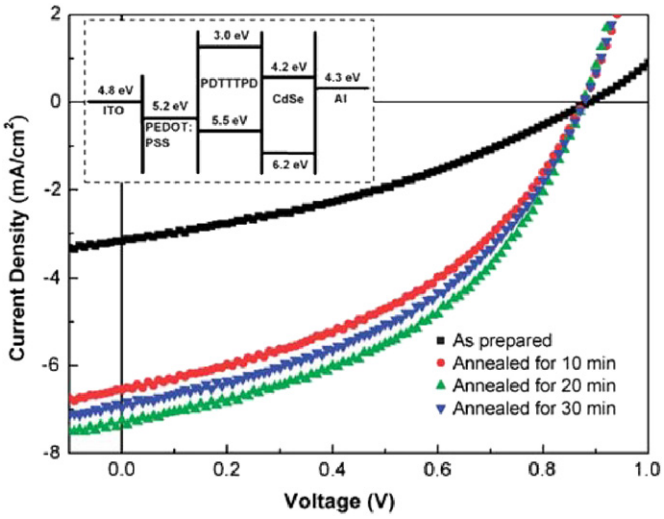

Fig. 18. Illuminated *J–V* characteristics displaying the impact of annealing on the electrical performance of the device. The inset displays the energy band diagram for the PDTTTPD:CdSe device [82].

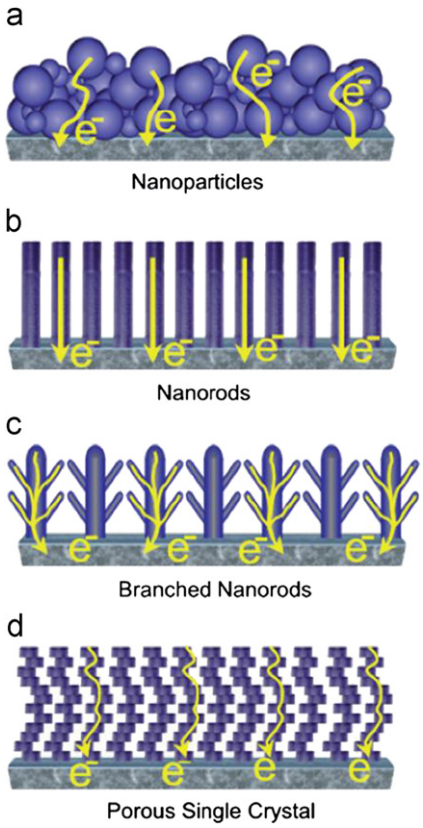

Fig. 19. Schematic representation of the possible nanostructured architectures for inorganic acceptor materials. Depicted are (a) quantum dots, (b) nanorods, (c) branched nanorods and (d) porous single crystal [26].

A post-production annealing process may also improve the nanomorphology of the device. Multiple reports suggest that for the donor material of P3HT, thermal treatments induce crystallinity in the polymer which can develop better conductive pathways and thus improve hole mobility [41,67,161]. This knowledge is somewhat transferrable to hybrid solar cells. Liu et al. optimised the performance of P3HT:Si NC hybrid solar cells by varying the thermal annealing temperature [75]. As more material combinations are explored, work towards optimising such parameters will become important, as the optimal conditions will vary to those of the commonly used P3HT:PCBM.

Kuo et al. also investigated the effect of thermal annealing on the active layer of a hybrid device. The authors used a blend consisting of the polymer PDTTTPD and CdSe tetrapods [82]. It was found that thermal annealing at a temperature of 130 °C for 20 min led to a significant increase in electrical performance. With reference to the as-prepared devices, the J_{sc} rose from 3.16 to 7.26 mA/cm^2 and the PCE rose from 1% to 2.9%. Fig. 18 displays the *J–V* characteristics for devices which have undergone thermal treatments at 130 °C, for varying time periods. It was thought that the annealing process caused an increase in performance by removing the pyridine ligands from the surface of the CdSe tetrapods, thus facilitating improved charge generation and collection. This was further evidenced by a reduction in peak intensity for the C–C and C–N vibrations measured by ATR-FTIR spectra. This indicates that the pyridine ligands, which were bound to the surface of the nanoparticle for the as-cast film, were removed by the thermal energy of annealing at 130 °C.

Importantly, this process was seen to influence the film nanomorphology. XRR analysis showed that the removal of surface pyridine led to a reduction in the inter-particle distance and thus an increase in CdSe packing density. TEM images also

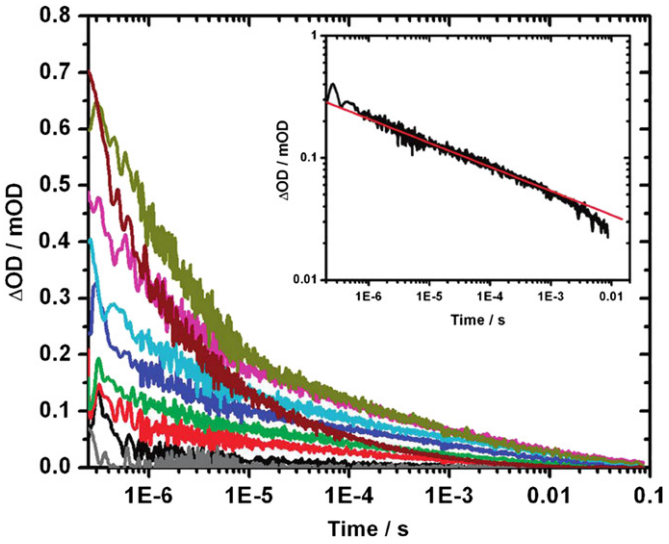

Fig. 20. Transient kinetics of a P3HT:CdS device for various weight composition ratios. The weight ratios investigated were 1:4 (red trace), 1:2 (green trace), 1.2:1 (dark blue trace), 2:1 (light blue trace), 3.1:1 (pink trace), 4.7:1 (dark yellow trace). A 1:1 ratio P3HT:PCBM film (dark red trace) is also displayed [96]. (For interpretation of the references to color in this figure legend, the reader is reffered to the web version of this article.)

suggested a reduction in inter-particle distance. This aggregation of CdSe was presumed to lead to improved electron transport, which consequently caused better electrical performance

Another approach to successfully control the nanomorphology is to grow vertically well-aligned nanostructures. Control over the physical dimensions of such structures can allow for a large D–A interfacial area as well as highly efficient electron transport. The II–VI semiconductor ZnO has recently become very attractive as an inorganic material to be used as a vertically aligned structure, as it can be formed using a variety of synthesis methods and exhibits high electron mobilities [26]. Even though this route could potentially lead to highly efficient bulk heterojunctions with near optimal designs, high PCEs have not been recorded with such a structure. The major limitation of these structures appears to be related to both the formation of a large surface area and the ability to properly infiltrate the polymer into the structure. Fig. 19 displays multiple possibilities for nanostructuring the inorganic acceptor material to improve the conducting pathways for electrons.

4. Emerging characterisation techniques

4.1. Transient absorption spectroscopy

Understanding the mechanisms of charge generation and recombination is crucial to allow significant improvement in device efficiency. Techniques using optical spectroscopy, such as transient absorption spectroscopy (TAS), may be used to study the nature of excited states in hybrid solar cells [162]. This technique is particularly useful as it can monitor all steps of device operation, being absorption, exciton diffusion and dissociation, charge transport and charge collection [163]. TAS is a pump probe spectroscopic technique which monitors changes in absorption caused by a laser induced photoexcitation. This time-resolved technique can monitor over a very large time range, which is crucial to provide a deep quantitative understanding of generation and recombination phenomena. Recent examples from literature utlilise this technique to observe the effect of both environmental screening and nanomorphological structure on the charge separation efficiency in organic photovoltaics [163]. Leventis et al. used TAS to investigate

recombination mechanisms in P3HT:CdS hybrid solar cells, as a function of CdS weight ratio [96]. This analysis is displayed in Fig. 20. The magnitude of the signal, which corresponds to the magnitude of change in optical density, is related to the number of photogenerated charge pairs. Increasing the weight ratio of CdS leads to an increase in charge generation yield. This study has shown that a weight ratio of 4.7:1 (CdS:P3HT) provides optimal charge photogeneration. Herrmann et al. used a TAS setup to investigate charge generation and recombination in P3HT:Si NC hybrid solar cells. The apparatus used was particularly novel, as it has a time resolution of 40 ps, and can measure over the entire spectral range from 415 to 1150 nm [131]. This set-up aims at overcoming experimental limits, relating to both time resolution and wavelength range, which have previously hindered efforts to investigate the fundamental mechanisms governing hybrid solar cells. This method was used to reveal ultrafast electron transfer from P3HT to Si NCs, suggesting that the material combination of P3HT:Si NCs is quite promising.

An improved understanding of recombination kinetics via studies using time resolved optical spectroscopy could allow a quicker transition to higher efficiencies, eliminating the dependence on trial and error optimisation of film composition and structure.

4.2. Conductive AFM (C-AFM)

The performance of bulk heterojunction devices depends heavily on the nanomorphology of the active layer. This refers to the size and spatial distribution of the donor and acceptor phases. There exists a delicate interplay between a large interfacial area within the active layer, and the need to provide sufficient conducting pathways for charge transport. To achieve the potential of solution processed devices, it is crucial to understand and optimise this aspect, to find some optimal compromise.

Traditional characterisation techniques of surface atomic force microscopy (AFM) coupled with *I–V* measurements have limited potential to provide deep understanding of the relationship between nanomorphology and device performance, as there are many interrelated variables which effect PCE.

Conductive AFM (C-AFM) is a technique which measures surface topography and local electronic characteristics simultaneously. It does this via a metal coated AFM probe which is connected to an external circuit. The simultaneous measurement of these two properties provides a direct link between D–A arrangement and electronic characteristics [164].

Dante et al. utilised this technique to investigate the effect of annealing on P3HT:PCBM films [165]. Fig. 21 displays cross sectional phase and hole current images of both as-cast (a,c) and thermally annealed (b,d) P3HT:PCBM samples. This analysis shows that the size of the P3HT domains increases and the two domains are more uniformly distributed as a result of the thermal treatment. This correlates to an increase in the high current regions in the hole current image for the annealed sample. The authors concluded that improved device performance was due to improved nanoscale ordering and increased charge carrier mobility. The ability for C-AFM to provide a direct link between nanomorphology and electronic performance makes it a viable tool for characterisation of heterojunction active layers, which makes it very appropriate for hybrid solar cells.

4.3. Electron tomography

The three dimensional organisation of donor and acceptor phases is very important for determining the excitonic dissociation, charge transport and thus PCE of a hybrid device. An in-depth understanding of this arrangement is required for efficient optimisation; however, to date, there is limited existence of tools to study the

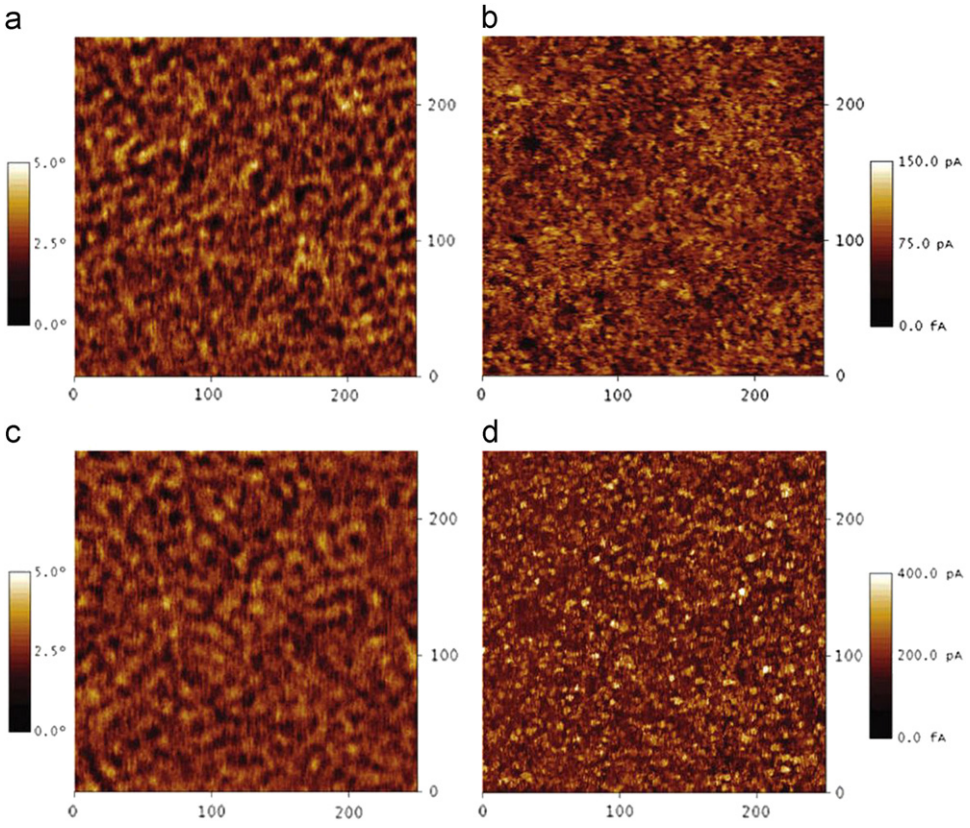

Fig. 21. Cross-section C-AFM images displaying phase (left) and hole current (right) for both as-cast (a) and (c) and thermally annealed (b) and (d) P3HT:PCBM films. All images are 250 nm × 250 nm. The bottom side of the image represents the side of the film closest to the ITO [165].

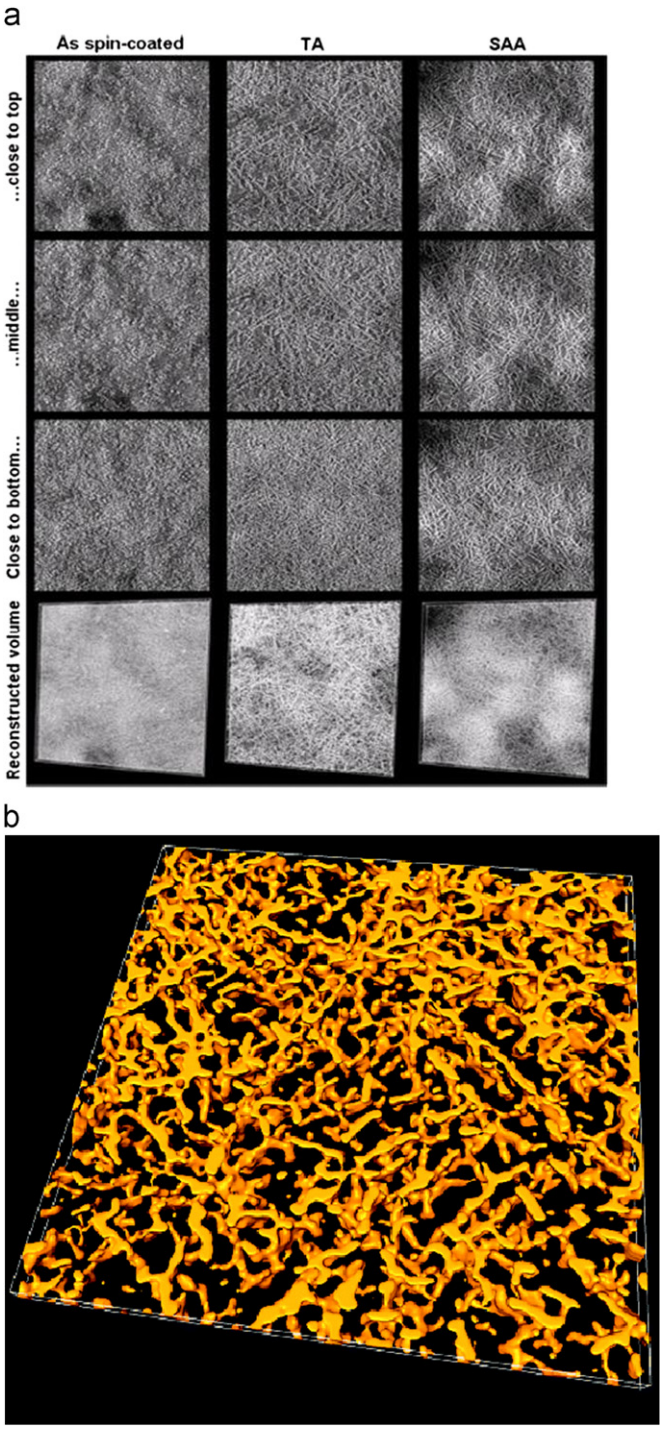

Fig. 22. (a) Results of electron tomography for P3HT:PCBM films. The three columns represent films which are as-cast, thermally annealed and solvent assisted annealed (left to right). The first three rows display 2D slices (x,y), measured at different heights (z). The final row represents a 3D reconstruction, formed by adding 2D data from individual slices. The scale of the images is 1700 nm × 1700 nm [166], (b) Electron tomography of a P3HT:ZnO sample. ZnO appears yellow whilst P3HT appears transparent [80]. (For interpretation of the references to color in this figure legend, the reader is reffered to the web version of this article.)

volumetric arrangement of the two phases. Both surface AFM measurements and cross sectional TEM are used, however, they only display information of a small 2D snapshot of the film, which provides only very limited structural information.

The technique of electron tomography may be able to provide this link between 3D spatial organisation and performance. This technique synthesises a series of 2D projections of TEM micrographs, taken at varying tilt angles, into a 3D, volumetric representation of the materials in the film [166]. This is performed by a software package which produces an array of voxels. This technique can assist in identifying the important morphology parameters which lead to desirable electronic characteristics.

Bavel et al. used this technique to investigate the effect of both thermal and solvent assisted annealing on P3HT:PCBM active layers [166]. Their findings are shown in Fig. 22(a). This displays individual slices of TEM for different scanning angles, which correspond to different depths within the film. The final row shows snapshots of reconstructed volumes of the three different devices. The authors show that the process of annealing has, in fact, formed crystalline 3D networks, when compared to the relatively amorphous as-cast layer. Additionally, desirable vertical phase separation is shown to occur, which causes the PCE to increase from 2% (as-cast) to 3.8% for both solvent assisted annealing and thermal annealing.

This technique is very applicable to hybrid films, due to the larger difference in electron density of conjugated polymers and inorganic nanoparticles. This will provide the ability to successfully construct a volumetric representation of a hybrid film, in which the donor and acceptor phases are accurately distinguished. A recent paper, published by Oosterhout et al., displays such a representation for a P3HT:ZnO hybrid solar cell. Fig. 22 b) displays a reconstructed volume of a P3HT:ZnO photoactive layer, obtained by electron tomography [80].

4.4. Kelvin probe microscopy

Kelvin probe microscopy (KPM) is a scanning probe technique used to measure surface potentiometry of a film. Currently used techniques of ultraviolet photoelectron spectroscopy (UPS) and X-ray photoelectron spectroscopy (XPS) cannot always be employed due to the relatively high resistance of the organic material. They also do not provide a direct link between surface voltage profile and topography. This apparatus operates in tapping mode, in a similar fashion to AFM, however, the tip-sample distance is increased. This

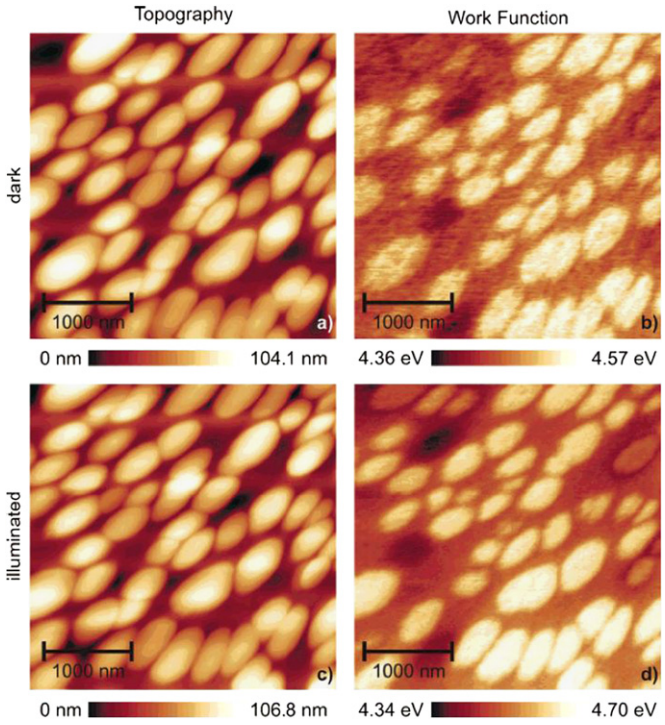

Fig. 23. Topography (left) and work function (right) of a toluene cast blend of MDMO-PPV:PCBM with a mass ratio of 1:4. Displayed are both dark (top row) and illuminated under a 442 nm cw laser (bottom row) [167].

separation makes the oscillations sensitive to long range electrostatic forces. The gradient of such forces is related to the potential difference between the tip and the sample [167,168]. Thus, unlike C-AFM, this technique measures an electrostatic interaction between two objects rather than a direct current flow [169]. As there is no contact between the tip and sample, this technique is well suited to soft materials, such as conjugated polymers. It also requires no sample preparation and produces high resolution spatial and voltage information, meaning this technique is very useful for analysing the relationship between film structure and work function.

Hoppe et al. used KPM to study the surface energetics of an organic solar cell consisting of MDMO-PPV:PCBM. The primary aim of this investigation was to identify differences in film properties as a result of using different solvents, namely toluene or chlorobenzene [167]. Electron transmission from the PCBM acceptor to the cathode was analysed and it was established that there existed some morphological barrier for this process in films cast using toluene as the solvent. The plot of surface topography and work function before and after illumination is displayed in Fig. 23. This provides evidence that the formation of appropriate percolated pathways for both electrons and holes is required for the successful operation of the device. More recently, Spadafora et al. demonstrated KPM with potentiometric lateral resolution on a sub-10 nm scale [83]. The excellent resolution was achieved by optimisation of the damping signal, which occurs due to the dissipation of energy during tip-sample interactions. Phase separation and electronic properties of optimised P3HT:PCBM solar cells were simultaneously monitored with excellent resolution. Under illumination, the lateral extension of the space charge area at the D–A interface was investigated, providing useful topographical information about the blend. Although this technique affords remarkable resolution in determining topographic and potentiometric information, the apparatus requires ultrahigh vacuum (UHV) conditions, as contamination significantly reduces accuracy [170].

5. Discussions

There are a number of issues which must be understood and overcome before the potential of this technology can be realised.

First, it is imperative to find the most optimal combination of organic and inorganic materials for hybrid solar cells. This requires careful consideration of the size of the individual material band gaps, which affects the range of absorption and thus maximum obtainable J_{sc}, and the diagonal band gap of the heterojunction, which determines the maximum obtainable V_{oc}. Additionally the ground state and excited state offsets, which govern the ability for both polymer and inorganic nanoparticle to dissociate excitons, must be considered. Advances in polymer chemistry are leading to breakthrough, new low band gap polymers which can achieve improved spectral response whilst still allowing for a large V_{oc}. The ideal electronic structure of the inorganic material is thought to be a band gap of $\sim$1.5 eV, with a HOMO level offset of $\sim$0.3 eV to allow for successful dissociation of excitons formed in the inorganic component. These characteristics are related to both the bulk band gap of the material, as well as the degree of quantum confinement, as determined by the physical geometry of the nanoparticles.

Advances in the synthetic processes used to form the inorganic material are required. Reproducible, well ordered structures are vital for the optimisation of the photoactive layer; however, these structures must be fabricated using techniques which are easily scalable. Additionally, a precise control over the physical geometry of the nanoparticle is needed to tailor and optimise the electronic structure.

One crucial aspect is the surface chemistry of the inorganic nanoparticles. The organic ligand which is attached to the surface of the nanoparticle during synthesis must be treated to ensure efficient charge transport. This surface chemistry may be favourably altered by an exchange of the thick insulating ligand with a more conductive molecule, such as pyridine; however, this is not necessarily ideal. Novel, simple techniques, such as acid treatments or thermal annealing must be developed to allow the improved charge transport properties of inorganic nanoparticles to be utilised within a hybrid device. Alternatively, *in situ* growth of the inorganic phase can eliminate the requirement of surface treatments; however, if this is to be a long term solution, it must too be compatible with high throughput processing.

Linked to the surface chemistry of the nanoparticle is the nanomorphology of the photoactive layer. It is very important that a balance between interfacial area and continuous conducting pathways is maintained within the photoactive layer. This may be achieved by vertical nanostructures of inorganic nanorods or nanowires, which act as the electron acceptor. Physically fabricating these structures poses many engineering challenges, perhaps the primary challenge being related to the physical dimensions demanded of photoactive layer, due to the excitonic diffusion length in typical conjugated polymers. For hybrid solar cells utilising nanocrystals or tetrapods dispersed in a polymer matrix, the composition of the solvents used play a large role in determining the film nanomorphology.

An improved understanding of the fundamental principles governing the operation of hybrid solar cells is required to efficiently and effectively increase device performance. This can be provided by new advanced characterisation techniques such as C-AFM and electron tomography.

The points raised above describe important future research required to increase the PCE of hybrid solar cells. Whilst PCE is vitally important, it should not be the sole consideration of researchers in the field. Fast, cheap processing is used as the main justification for this technology; however, little research is yet to focus on fabrication and processing. Before organic–inorganic hybrid solar cells can be considered convincing, demonstration of high volume production is necessary. Additionally, the associated costs of the fabrication process must be understood [171]. Until such research is conducted, the technology can be considered no more than a scientific curiosity. Preliminary investigations exploring these concerns have been performed recently for OPV devices [7,14,15,172]. A further aspect for consideration is the environmental stability of the device/module [47,48,173]. Such investigations will be important in determining the commercial viability of this technology, which is, ultimately, the most important consideration.

Table 2 displays a concise description of current understanding of commercial aspects associated with this technology. It aims to give a comparison of the suitability for commercial production of the four inorganic material groups surveyed in this article.

Silicon is a non-toxic element. Metal oxide semiconductors, some of which are used in consumer products such as sunscreen, paint and toothpaste, are generally considered non-toxic [174].

Table 2
A simple table describing the suitability of the four discussed material groups for commercialisation, considering key aspects. A+indicates suitability for that aspect, whilst a—indicates the material is not suitable/requires further investigation regarding that aspect.

Inorganic nanoparticle	Non-toxic	Abundance	Lifetime	Potential processing speed
Cadmium compounds (CdSe, CdTe)	–	–	–	+
Silicon	+	+	No data	+
Metal oxides (TiO_2, ZnO)	+	+	No data	–
Low band gap (PbS, PbSe, $CuInSe_2$)	–	–	No data	+

Cadmium based compounds are inherently toxic, as are low band gap materials containing lead (e.g., PbS). Whilst varying levels of toxicity may exist within the different discussed material groups, there is still conjecture regarding the health hazards associated with inorganic nanomaterials. Multiple reports have suggested that inhalation of nanoparticles can lead to health problems, not only to the respiratory system, but also the circulatory system and other organs [175]. This is a processing issue which must be appropriately addressed before manufacturing of this technology can be accelerated. One issue regarding toxicity of processing steps, aside from the materials alone, is the reliance on chlorinated solvents [176]. Environmentally friendly alternatives must be found. Dong et al. recently demonstrated an all-water-solution processed organic–inorganic hybrid solar cell [177]. Poly(phenylene vinylene) (PPV) was used as the donor material and anatase TiO_2 was used as the electron acceptor. Although the hybrid device only achieved a PCE of 0.11%, demonstration of using water as the processing solvent represents a necessary, environmentally friendly alternative to previous solvents.

To ensure sustainable growth of photovoltaics as an energy source, the abundance of the materials used must be considered [178,179]. In order to meet predicted increases in energy demand, it has been suggested that 1 GW_p of daily production on a global level is required [2]. Whilst it is difficult to quantify the possible volume of production for semiconductor nanoparticles, availability of raw materials gives some indication of the suitability of a material to meet the requirement of significant upscaling of production. An excellent resource for such data is the U.S. Geological survey, Mineral commodity summaries [180]. Concerning inorganic semiconductors for hybrid solar cells, silicon is the most abundant. Some elements commonly used in photovoltaics have constraints on their availability, which could limit their suitability for large scale production. Tellurium and indium are two such elements. These are used in the compounds CdTe and $CuInSe_2$. To meet upscaled production, which addresses predicted increases in energy demand, semiconductors using these materials should be avoided. Another concern regarding the availability of indium is the production of ITO, the transparent conducting oxide used as the anode for OPV and hybrid devices. Indium is the main constituent of ITO. Whilst ITO provides an effective trade-off between transparency and high conductivity, future development of the technology requires an alternative. Several methods of device fabrication which do not require an ITO layer have been demonstrated [181,182].

The lifetime of organic–inorganic hybrid solar cells is key to the success of the technology, as it has a large influence on investor confidence and consumer interest. Hybrid solar cells could theoretically achieve improved stability when compared to OPV. One major hurdle for bulk heterojunction organic solar cells, which use fullerenes as the electron acceptor, is the instability of the metastable structure of the photoactive layer [183]. This structure is prone to reorganisation as a consequence of elevated temperatures, or even after time at ambient temperature, often leading to reduced performance. This is caused by the movement of PCBM, which tends to form aggregates [184]. The replacement of PCBM with an inorganic nanoparticle may allow for more stable structures in the photoactive layer. Within literature, almost no data exists regarding empirical lifetimes of hybrid solar cells. One of the first reports of this kind was published by Dayal et al. The authors showed that after storing a PCPDTBT:CdSe hybrid device in a glovebox in an N_2 atmosphere for 3 months, the PCE was still over 3%, which exceeds 90% of the devices initial PCE [21]. However promising, these conditions do not represent those experienced in real world applications. Yang et al. demonstrated an improvement in stability of P3HT:CdSe devices by incorporating a ZnO layer between the active layer and the cathode [185]. The lifetime of these devices, without a ZnO layer, in ambient air, without encapsulation is said to be very short. With a ZnO layer, the device efficiency remained at 70% after exposure to ambient laboratory conditions for 75 day. The cause of this improvement in device stability is believed to be related to a reduction in oxidation of the polymer, as oxygen and water molecules are blocked by the ZnO nanocrystal layer. It is evident from the small body of existing literature that device stability for hybrid solar cells is a pressing concern, and that modifications to the conventional structure are necessary.

Many laboratory reports have reported high efficiencies for small area devices, using batch processing methods such as spin coating and thermal evaporation. The next challenge for this growing field of research is to demonstrate the previously assumed ability of producing large area solar cells using high throughput, low cost fabrication techniques. This is a particularly challenging prospect, as there are multiple different possible printing techniques which could be employed to achieve this goal [176,186]. Additionally, the delicate dependence between the many processing parameters affiliated with laboratory scale device production, which has been heavily investigated, is not necessarily transferable to large scale production. Research must be directed at discovering optimal processing parameters, particularly for coating and drying of layers within the device. The first such investigation was reported by Wengeler et al., whereby the authors demonstrated the preparation of knife and slot die coated hybrid solar cells. P3HT:quantum dot solar cells with a PCE of 1.18% were produced using the knife coating technique, which represents an impressive first step [187]. The impact of drying conditions on cell performance was investigated. It was shown that lower drying airflow yields higher current density and thus higher PCE. All inorganic materials discussed in this article, except for well-aligned metal oxide nanoparticles, would be compatible with high throughput coating methods to produce hybrid devices, as described by Wengeler et al., as they are normally dispersed within a polymer matrix by coating from a solution. The fabrication of vertically well-aligned nanostructures using metal oxides, with optimised physical dimensions, may provide benefits to the operation of the device; however, producing such a structure using methods compatible with roll-to-roll processing is a daunting task, which requires intensive process engineering efforts.

Another important consideration is the energy embodied in the solar cell during manufacturing processes. Multiple reports concerning life cycle analysis exist for OPV devices [188,189]. These reports paint a relatively positive picture, suggesting that the environmental impact associated with high throughput, low cost fabrication of organic solar cells is low. An initial life cycle analysis considering hybrid solar cells was recently reported [190]. This report focusses exclusively on laboratory-based fabrication techniques, not roll-to-roll methods. It too concludes with a positive outlook; however, it is shown that degradation of efficiency has a large impact on the sustainability of this technology. A more comprehensive study, including data for commercial scale production is required to establish research areas which require critical attention.

6. Conclusion

The costs benefits associated with using organic materials for photovoltaic devices could render OPV as a viable source of renewable energy. The addition of an inorganic acceptor material to form an organic–inorganic hybrid solar cell should theoretically improve the performance of OPV, due to additional advantages such as enhanced absorption and improved charge transport characteristics. However, to date, the efficiency of hybrid solar cells have been very low, when compared to their all-organic counterparts.

There are some design considerations when choosing an appropriate inorganic material. It has been identified that an optimal electronic design for such a material would be a band gap of 1.5 eV and a HOMO level offset of 0.3 eV to allow both a significant absorption contribution as well as a large V_{oc}. There exist, however, additional physical considerations which must be taken into account when choosing an appropriate material. The different materials which have thus far been considered have both advantages and disadvantages, however, no material has been coupled with a polymer to provide electrical performance superior to that of an OPV device, for which PCEs of 10% have been achieved. The major limitation to device performance is related to the effect of the insulating surface ligand on the electrical performance of the nanoparticles. New treatments aimed at reducing this negative effect show promise to realise the potential of this technology. Another drawback associated with the addition of an inorganic material is the seemingly non- ideal nanomorphology of a hybrid structure. A deeper understanding of this property, as well as that of the fundamental mechanisms determining the operation of hybrid solar cells is required to efficiently and effectively increase device performance. This can be provided by new advanced characterisation techniques such as Conductive AFM and transient absorption spectroscopy. Improvements which allow the full potential of hybrid solar cells to be realised could render this technology a very competitive, clean source of energy for the future.

Acknowledgements

This work was produced with the financial assistance of the Australian Research Council. The authors would like to thank Xiaohan Yang, Gavin Conibeer, Mattias Juhl and Thilini Ishwara for useful scientific discussions and guidance.

References

[1] M.A. Green, K. Emery, Y. Hishikawa, W. Warta, E.D. Dunlop, Solar cell efficiency tables (version 39), Progress in Photovoltaics: Research and Applications 20 (2012) 12–20.
[2] N. Espinosa, M. Hosel, D. Angmo, F.C. Krebs, Solar cells with one-day energy payback for the factories of the future, Energy & Environmental Science 5 (2012) 5117–5132.
[3] C.J. Brabec, Organic photovoltaics: technology and market, Solar Energy Materials and Solar Cells 83 (2004) 273–292.
[4] B.R. Saunders, M.L. Turner, Nanoparticle-polymer photovoltaic cells, Advances in Colloid and Interface Science 138 (2008) 1–23.
[5] P. Jackson, D. Hariskos, E. Lotter, S. Paetel, R. Wuerz, R. Menner, W. Wischmann, M. Powalla, New world record efficiency for Cu(In,Ga)Se2 thin-film solar cells beyond 20%, Progress in Photovoltaics: Research and Applications 19 (2011) 894–897.
[6] C.W. Tang, Two-layer organic photovoltaic cell, Applied Physics Letters 48 (1986) 183–185.
[7] K. Frederik C, Fabrication and processing of polymer solar cells: a review of printing and coating techniques, Solar Energy Materials and Solar Cells 93 (2009) 394–412.
[8] T.T. Larsen-Olsen, B. Andreasen, T.R. Andersen, A.P.L. Böttiger, E. Bundgaard, K. Norrman, J.W. Andreasen, M. Jørgensen, F.C. Krebs, Simultaneous multilayer formation of the polymer solar cell stack using roll-to-roll double slot-die coating from water, Solar Energy Materials and Solar Cells 97 (2012) 22–27.
[9] U. Zhokhavets, T. Erb, G. Gobsch, M. Al-Ibrahim, O. Ambacher, Relation between absorption and crystallinity of poly(3-hexylthiophene)/fullerene films for plastic solar cells, Chemical Physics Letters 418 (2006) 347–350.
[10] H.-Y. Chen, J. Hou, S. Zhang, Y. Liang, G. Yang, Y. Yang, L. Yu, Y. Wu, G. Li, Polymer solar cells with enhanced open-circuit voltage and efficiency, Nature Photonics 3 (2009) 649–653.
[11] J. Peet, J.Y. Kim, N.E. Coates, W.L. Ma, D. Moses, A.J. Heeger, G.C. Bazan, Efficiency enhancement in low-Bandgap polymer solar cells by processing with alkane dithiols, Nature Materials 6 (2007) 497–500.
[12] R.F. Service, Outlook brightens for plastic solar cells, Science 332 (2011) 293.
[13] see 2012 press release, 〈www.heliatek.com〉.
[14] F.C. Krebs, M. Jørgensen, K. Norrman, O. Hagemann, J. Alstrup, T.D. Nielsen, J. Fyenbo, K. Larsen, J. Kristensen, A complete process for production of flexible large area polymer solar cells entirely using screen printing—First public demonstration, Solar Energy Materials and Solar Cells 93 (2009) 422–441.
[15] F.C. Krebs, T.D. Nielsen, J. Fyenbo, M. Wadstrom, M.S. Pedersen, Manufacture, integration and demonstration of polymer solar cells in a lamp for the Lighting Africa initiative, Energy & Environmental Science 3 (2010) 512–525.
[16] Y. Zhou, M. Eck, M. Kruger, Bulk-heterojunction hybrid solar cells based on colloidal nanocrystals and conjugated polymers, Energy & Environmental Science 3 (2010) 1851–1864.
[17] T. Xu, Q. Qiao, Conjugated polymer–inorganic semiconductor hybrid solar cells, Energy & Environmental Science 4 (2011) 2700–2720.
[18] S. Ren, L.-Y. Chang, S.-K. Lim, J. Zhao, M. Smith, N. Zhao, V. Bulovic, M. Bawendi, S. Gradečak, Inorganic–Organic hybrid solar cell: bridging quantum dots to conjugated polymer nanowires, Nano Letters 11 (2011) 3998–4002.
[19] Y. Zhou, M. Eck, C. Veit, B. Zimmermann, F. Rauscher, P. Niyamakom, S. Yilmaz, I. Dumsch, S. Allard, U. Scherf, M. Krüger, Efficiency enhancement for bulk-heterojunction hybrid solar cells based on acid treated CdSe quantum dots and low Bandgap polymer PCPDTBT, Solar Energy Materials and Solar Cells 95 (2011) 1232–1237.
[20] D. Celik, M. Krueger, C. Veit, H.F. Schleiermacher, B. Zimmermann, S. Allard, I. Dumsch, U. Scherf, F. Rauscher, P. Niyamakom, Performance enhancement of CdSe nanorod-polymer based hybrid solar cells utilizing a novel combination of post-synthetic nanoparticle surface treatments, Solar Energy Materials and Solar Cells 98 (2012) 433–440.
[21] S. Dayal, N. Kopidakis, D.C. Olson, D.S. Ginley, G. Rumbles, Photovoltaic devices with a low band Gap polymer and CdSe nanostructures exceeding 3% efficiency, Nano Letters 10 (2009) 239–242.
[22] N.C. Nicolaidis, B.S. Routley, J.L. Holdsworth, W.J. Belcher, X. Zhou, P.C. Dastoor, Fullerene contribution to photocurrent generation in organic photovoltaic cells, The Journal of Physical Chemistry C 115 (2011) 7801–7805.
[23] T. Takagahara, K. Takeda, Theory of the quantum confinement effect on excitons in quantum dots of indirect-gap materials, Physical Review B 46 (1992) 15578–15581.
[24] A. Guchhait, A.K. Rath, A.J. Pal, To make polymer: quantum dot hybrid solar cells NIR-active by increasing diameter of PbSnanoparticles, Solar Energy Materials and Solar Cells 95 (2011) 651–656.
[25] J. Huang, Z. Huang, Y. Yang, H. Zhu, T. Lian, Multiple exciton dissociation in CdSe quantum dots by ultrafast electron transfer to adsorbed methylene blue, Journal of the American Chemical Society 132 (2010) 4858–4864.
[26] I. Gonzalez-Valls, M. Lira-Cantu, Vertically-aligned nanostructures of ZnO for excitonic solar cells: a review, Energy & Environmental Science 2 (2009) 19–34.
[27] E. Marti´nez-Ferrero, J Albero, E. Palomares, Materials, nanomorphology, and interfacial charge transfer reactions in quantum dot/polymer solar cell devices, The Journal of Physical Chemistry Letters 1 (2010) 3039–3045.
[28] S. Brian R, Hybrid polymer/nanoparticle solar cells: preparation, principles and challenges, Journal of Colloid and Interface Science 369 (2012) 1–15.
[29] W. Cai, X. Gong, Y. Cao, Polymer solar cells: recent development and possible routes for improvement in the performance, Solar Energy Materials and Solar Cells 94 (2010) 114–127.
[30] G. Garcia-Belmonte, A. Munar, E.M. Barea, J. Bisquert, I. Ugarte, R. Pacios, Charge carrier mobility and lifetime of organic bulk heterojunctions analyzed by impedance spectroscopy, Organic Electronics 9 (2008) 847–851.
[31] C.J. Brabec, S. Gowrisanker, J.J.M. Halls, D. Laird, S. Jia, S.P. Williams, Polymer–Fullerene bulk-heterojunction solar cells, Advanced Materials 22 (2010) 3839–3856.
[32] N.S. Sariciftci, L. Smilowitz, A.J. Heeger, F. Wudl, Photoinduced electron transfer from a conducting polymer to Buckminsterfullerene, Science 258 (1992) 1474–1476.
[33] S.H. Park, A. Roy, S. Beaupre, S. Cho, N. Coates, J.S. Moon, D. Moses, M. Leclerc, K. Lee, A.J. Heeger, Bulk heterojunction solar cells with internal quantum efficiency approaching 100%, Nature Photonics 3 (2009) 297–302.
[34] G. Yu, J. Gao, J.C. Hummelen, F. Wudl, A.J. Heeger, Polymer photovoltaic cells: enhanced efficiencies via a network of internal donor–acceptor heterojunctions, Science 270 (1995) 1789–1791.
[35] E. Bundgaard, F.C. Krebs, Low band gap polymers for organic photovoltaics, Solar Energy Materials and Solar Cells 91 (2007) 954–985.
[36] E. Bundgaard, S.E. Shaheen, F.C. Krebs, D.S. Ginley, Bulk heterojunctions based on a low band gap copolymer of thiophene and benzothiadiazole, Solar Energy Materials and Solar Cells 91 (2007) 1631–1637.
[37] J. Hou, T.L. Chen, S. Zhang, H.-Y. Chen, Y. Yang, Poly[4,4-bis(2-ethylhexyl)cyclopenta[2,1-b;3,4-b′]dithiophene-2,6-diyl-alt-2,1,3- benzoselenadiazole-4,7-diyl], a new low band gap polymer in polymer solar cells, The Journal of Physical Chemistry C 113 (2009) 1601–1605.
[38] J. Hou, H.-Y. Chen, S. Zhang, G. Li, Y. Yang, Synthesis, characterization, and photovoltaic properties of a low band gap polymer based on silole-containing polythiophenes and 2,1,3-benzothiadiazole, Journal of the American Chemical Society 130 (2008) 16144–16145.
[39] J. Hou, H.-Y. Chen, S. Zhang, R.I. Chen, Y. Yang, Y. Wu, G. Li, Synthesis of a low band gap polymer and its application in highly efficient polymer solar cells, Journal of the American Chemical Society 131 (2009) 15586–15587.
[40] B.A. Gregg, M.C. Hanna, Comparing organic to inorganic photovoltaic cells: theory, experiment, and simulation, Journal of Applied Physics 93 (2003) 3605–3614.

[41] V.D. Mihailetchi, H.X. Xie, B. de Boer, L.J.A. Koster, P.W.M. Blom, Charge Transport and photocurrent generation in poly(3-hexylthiophene): methanofullerene bulk-heterojunction solar cells, Advanced Functional Materials 16 (2006) 699–708.
[42] H.-L. Yip, A.K.Y. Jen, Recent advances in solution-processed interfacial materials for efficient and stable polymer solar cells, Energy & Environmental Science 5 (2012) 5994–6011.
[43] L. Zuo, X. Jiang, M. Xu, L. Yang, Y. Nan, Q. Yan, H. Chen, Enhancement of short current density in polymer solar cells with phthalocyanine tin (IV) dichloride as interfacial layer, Solar Energy Materials and Solar Cells 95 (2011) 2664–2669.
[44] W.J. Potscavage, A. Sharma, B. Kippelen, Critical interfaces in organic solar cells and their influence on the open-circuit voltage, Accounts of Chemical Research 42 (2009) 1758–1767.
[45] J. Zhao, A. Wang, M.A. Green, 24·5% efficiency silicon PERT cells on MCZ substrates and 24·7% efficiency PERL cells on FZ substrates, Progress in Photovoltaics: Research and Applications 7 (1999) 471–474.
[46] D. Gupta, S. Mukhopadhyay, K.S. Narayan, Fill factor in organic solar cells, Solar Energy Materials and Solar Cells 94 (2010) 1309–1313.
[47] M. Jørgensen, K. Norrman, F.C. Krebs, Stability/degradation of polymer solar cells, Solar Energy Materials and Solar Cells 92 (2008) 686–714.
[48] D.M. Tanenbaum, H.F. Dam, R. Rösch, M. Jørgensen, H. Hoppe, F.C. Krebs, Edge sealing for low cost stability enhancement of roll-to-roll processed flexible polymer solar cell modules, Solar Energy Materials and Solar Cells 97 (2012) 157–163.
[49] C.J. Brabec, A. Cravino, D. Meissner, N.S. Sariciftci, T. Fromherz, M.T. Rispens, L. Sanchez, J.C. Hummelen, Origin of the open circuit voltage of plastic solar cells, Advanced Functional Materials 11 (2001) 374–380.
[50] M.C. Scharber, D. Mühlbacher, M. Koppe, P. Denk, C. Waldauf, A.J. Heeger, C.J. Brabec, Design rules for donors in bulk-heterojunction solar cells—towards 10% energy-conversion efficiency, Advanced Materials 18 (2006) 789–794.
[51] K. Vandewal, A. Gadisa, W.D. Oosterbaan, S. Bertho, F. Banishoeib, I. Van Severen, L. Lutsen, T.J. Cleij, D. Vanderzande, J.V. Manca, The relation between open-circuit voltage and the onset of photocurrent generation by charge-transfer absorption in polymer:fullerene bulk heterojunction solar cells, Advanced Functional Materials 18 (2008) 2064–2070.
[52] W. Shockley, H.J. Queisser, Detailed balance limit of efficiency of *p–n* junction solar cells, Journal of Applied Physics 32 (1961) 510–519.
[53] K. Vandewal, K. Tvingstedt, A. Gadisa, O. Inganas, J.V. Manca, On the origin of the open-circuit voltage of polymer-fullerene solar cells, Nature Materials 8 (2009) 904–909.
[54] T. Yamanari, T. Taima, J. Sakai, K. Saito, Origin of the open-circuit voltage of organic thin-film solar cells based on conjugated polymers, Solar Energy Materials and Solar Cells 93 (2009) 759–761.
[55] T. Ishwara, D.D. Bradley, J. Nelson, P. Ravirajan, I. Vanseveren, T. Cleij, D. Vanderzandee, L. Lusten, S. Tierney, M. Heeney, I McCulloch, Influence of polymer ionization potential on the open-circuit voltage of hybrid polymer/TiO_2 solar cells, Applied Physics Letters 92 (2008) 053308.
[56] J.E. Brandenburg, X. Jin, M. Kruszynska, J. Ohland, J. Kolny-Olesiak, I. Riedel, H. Borchert, J. Parisi, Influence of particle size in hybrid solar cells composed of CdSe nanocrystals and poly(3-hexylthiophene), Journal of Applied Physics 110 (2011) 064509–064509.
[57] S.E. Shaheen, C.J. Brabec, N.S. Sariciftci, F. Padinger, T. Fromherz, J.C. Hummelen, 2.5% efficient organic plastic solar cells, Applied Physics Letters 78 (2001) 841–843.
[58] G. Dennler, M.C. Scharber, C.J. Brabec, Polymer–Fullerene bulk-heterojunction solar cells, Advanced Materials 21 (2009) 1323–1338.
[59] X. Yang, J. Loos, S.C. Veenstra, W.J.H. Verhees, M.M. Wienk, J.M. Kroon, M.A.J. Michels, R.A.J. Janssen, Nanoscale morphology of high-performance polymer solar cells, Nano Letters 5 (2005) 579–583.
[60] M.T. Dang, G. Wantz, H. Bejbouji, M. Urien, O.J. Dautel, L. Vignau, L. Hirsch, Polymeric solar cells based on P3HT:PCBM: role of the casting solvent, Solar Energy Materials and Solar Cells 95 (2011) 3408–3418.
[61] L. Chang, H.W.A. Lademann, J.-B. Bonekamp, K. Meerholz, A.J. Moulé, Effect of trace solvent on the morphology of P3HT:PCBM bulk heterojunction solar cells, Advanced Functional Materials 21 (2011) 1779–1787.
[62] D. Chirvase, J. Parisi, J.C. Hummelen, V. Dyakonov, Influence of nanomorphology on the photovoltaic action of polymer–fullerene composites, Nanotechnology 15 (2004) 1317.
[63] W.-H. Baek, H. Yang, T.-S. Yoon, C.J. Kang, H.H. Lee, Y.-S. Kim, Effect of P3HT:PCBM concentration in solvent on performances of organic solar cells, Solar Energy Materials and Solar Cells 93 (2009) 1263–1267.
[64] A.J. Morfa, K.L. Rowlen, T.H. Reilly, M.J. Iii, J. Romero, van de Lagemaat, Plasmon-enhanced solar energy conversion in organic bulk heterojunction photovoltaics, Applied Physics Letters 92 (2008) 013503–013504.
[65] H.A. Atwater, A. Polman, Plasmonics for improved photovoltaic devices, Nature Materials 9 (2010) 205–213.
[66] X. Yang, A. Uddin, M. Wright, Plasmon enhanced light absorption in bulk heterojunction organic solar cells, physica status solidi (RRL)—Rapid Research Letters 6 (2012) 199–201.
[67] W. Ma, C. Yang, X. Gong, K. Lee, A.J. Heeger, Thermally Stable, Efficient polymer solar cells with nanoscale control of the interpenetrating network morphology, Advanced Functional Materials 15 (2005) 1617–1622.
[68] K. Kim, J. Liu, M.A.G. Namboothiry, D.L. Carroll, Roles of donor and acceptor nanodomains in 6% efficient thermally annealed polymer photovoltaics, Applied Physics Letters 90 (2007) 163511–163513.
[69] G. Li, V. Shrotriya, J. Huang, Y. Yao, T. Moriarty, K. Emery, Y. Yang, High-efficiency solution processable polymer photovoltaic cells by self-organization of polymer blends, Nature Materials 4 (2005) 864–868.
[70] F.-C. Chen, C.-J. Ko, J.-L. Wu, W.-C. Chen, Morphological study of P3HT:PCBM blend films prepared through solvent annealing for solar cell applications, Solar Energy Materials and Solar Cells 94 (2010) 2426–2430.
[71] Z. He, C. Zhong, X. Huang, W.-Y. Wong, H. Wu, L. Chen, S. Su, Y. Cao, Simultaneous enhancement of open-circuit voltage, short-circuit current density, and fill factor in polymer solar cells, Advanced Materials 23 (2011) 4636–4643.
[72] Y. Liang, Z. Xu, J. Xia, S.-T. Tsai, Y. Wu, G. Li, C. Ray, L. Yu, For the bright future—bulk heterojunction polymer solar cells with power conversion efficiency of 7.4%, Advanced Materials 22 (2010) E135–E138.
[73] M. Helgesen, R. Sondergaard, F.C. Krebs, Advanced materials and processes for polymer solar cell devices, Journal of Materials Chemistry 20 (2010).
[74] H. Borchert, Elementary processes and limiting factors in hybrid polymer/nanoparticle solar cells, Energy & Environmental Science 3 (2010) 1682–1694.
[75] C.-Y. Liu, Z.C. Holman, U.R. Kortshagen, Optimization of Si NC/P3HT hybrid solar cells, Advanced Functional Materials 20 (2010) 2157–2164.
[76] A.P. Alivisatos, Semiconductor clusters, nanocrystals, and quantum dots, Science 271 (1996) 933–937.
[77] H. Xiang, S.-H. Wei, X. Gong, Identifying optimal inorganic nanomaterials for hybrid solar cells, The Journal of Physical Chemistry C 113 (2009) 18968–18972.
[78] H.-C. Chen, C.-W. Lai, I.C. Wu, H.-R. Pan, I.W.P. Chen, Y.-K. Peng, C.-L. Liu, C.-h. Chen, P.-T. Chou, Enhanced performance and air stability of 3.2% hybrid solar cells: how the functional polymer and CdTe nanostructure boost the solar cell efficiency, Advanced Materials 23 (2011) 5451–5455.
[79] T. Krishnamoorthy, V. Thavasi, M. Subodh, G, S. Ramakrishna, A first report on the fabrication of vertically aligned anatase TiO_2 nanowires by electrospinning: preferred architecture for nanostructured solar cells, Energy & Environmental Science 4 (2011).
[80] S.D. Oosterhout, M.M. Wienk, S.S. van Bavel, R. Thiedmann, L. Jan Anton Koster, J. Gilot, J. Loos, V. Schmidt, R.A.J. Janssen, The effect of three-dimensional morphology on the efficiency of hybrid polymer solar cells, Nature Materials 8 (2009) 818–824.
[81] M. Bredol, K. Matras, A. Szatkowski, J. Sanetra, A. Prodi-Schwab, P3HT/ZnS: a new hybrid bulk heterojunction photovoltaic system with very high open circuit voltage, Solar Energy Materials and Solar Cells 93 (2009) 662–666.
[82] C.-Y. Kuo, M.-S. Su, G.-Y. Chen, C.-S. Ku, H.-Y. Lee, K.-H. Wei, Annealing treatment improves the morphology and performance of photovoltaic devices prepared from thieno[3,4-c]pyrrole-4,6-dione-based donor/acceptor conjugated polymers and CdSe nanostructures, Energy & Environmental Science 4 (2011) 2316–2322.
[83] E.J. Spadafora, R. Demadrille, B. Ratier, B. Gre´vin, Imaging the carrier photogeneration in nanoscale phase segregated organic heterojunctions by kelvin probe force microscopy, Nano Letters 10 (2010) 3337–3342.
[84] M. Koppe, H.-J. Egelhaaf, G. Dennler, M.C. Scharber, C.J. Brabec, P. Schilinsky, C.N. Hoth, Near IR sensitization of organic bulk heterojunction solar cells: towards optimization of the spectral response of organic solar cells, Advanced Functional Materials 20 (2010) 338–346.
[85] J.Y. Kim, K. Lee, N.E. Coates, D. Moses, T.-Q. Nguyen, M. Dante, A.J. Heeger, Efficient tandem polymer solar cells fabricated by all-solution processing, Science 317 (2007) 222–225.
[86] J. Jasieniak, M. Califano, S.E. Watkins, Size-dependent valence and conduction band-edge energies of semiconductor nanocrystals, ACS Nano 5 (2011) 5888–5902.
[87] L. He, Highly efficient Si-nanorods/organic hybrid core-sheath heterojunction solar cells, Applied Physics Letters 99 (2011) 021104.
[88] C.-Y. Liu, Z.C. Holman, U.R. Kortshagen, Hybrid solar cells from P3HT and silicon nanocrystals, Nano Letters 9 (2008) 449–452.
[89] C.Y. Kuo, W.C. Tang, C. Gau, T.F. Guo, D.Z. Jeng, Ordered bulk heterojunction solar cells with vertically aligned TiO_2 nanorods embedded in a conjugated polymer, Applied Physics Letters 93 (2008) 033303–033307.
[90] W. Chen, Y. Chen, F. Li, L. Chen, K. Yuan, K. Yao, P. Wang, Ordered microstructure induced by orientation behavior of liquid-crystal polythiophene for performance improvement of hybrid solar cells, Solar Energy Materials and Solar Cells 96 (2012) 266–275.
[91] M.P. Mikhailova, A.N. Titkov, Type II heterojunctions in the GaInAsSb/GaSb system, Semiconductor Science and Technology 9 (1994) 1279.
[92] S. Dowland, T. Lutz, A. Ward, S.P. King, A. Sudlow, M.S. Hill, K.C. Molloy, S.A. Haque, Direct growth of metal sulfide nanoparticle networks in solid-state polymer films for hybrid inorganic–organic solar cells, Advanced Materials 23 (2011) 2739–2744.
[93] W.-C. Kwak, T.G. Kim, W. Lee, S.-H. Han, Y.-M. Sung, Template-free liquid-phase synthesis of high-density CdS nanowire arrays on conductive glass, The Journal of Physical Chemistry C 113 (2009) 1615–1619.
[94] L. Wang, Y. Liu, X. Jiang, D. Qin, Y. Cao, Enhancement of photovoltaic characteristics using a suitable solvent in hybrid polymer/multiarmed CdS nanorods solar cells, The Journal of Physical Chemistry C 111 (2007) 9538–9542.
[95] M. Zhong, D. Yang, J. Zhang, J. Shi, X. Wang, C. Li, Improving the performance of CdS/P3HT hybrid inverted solar cells by interfacial modification, Solar Energy Materials and Solar Cells 96 (2012) 160–165.

[96] H.C. Leventis, S.P. King, A. Sudlow, M.S. Hill, K.C. Molloy, S.A. Haque, Nanostructured hybrid polymer–inorganic solar cell active layers formed by controllable *in Situ* growth of semiconducting sulfide networks, Nano Letters 10 (2010) 1253–1258.
[97] K.F. Jeltsch, M. Schädel, J.-B. Bonekamp, P. Niyamakom, F. Rauscher, H.W.A. Lademann, I. Dumsch, S. Allard, U. Scherf, K. Meerholz, Efficiency enhanced hybrid solar cells using a blend of quantum dots and nanorods, Advanced Functional Materials 22 (2012) 397–404.
[98] R. Zhou, Y. Zheng, L. Qian, Y. Yang, P.H. Holloway, J. Xue, Solution-processed, nanostructured hybrid solar cells with broad spectral sensitivity and stability, Nanoscale 4 (2012) 3507–3514.
[99] Y. Zhou, M. Eck, C. Men, F. Rauscher, P. Niyamakom, S. Yilmaz, I. Dumsch, S. Allard, U. Scherf, M. Krüger, Efficient polymer nanocrystal hybrid solar cells by improved nanocrystal composition, Solar Energy Materials and Solar Cells 95 (2011) 3227–3232.
[100] B. Sun, N.C. Greenham, Improved efficiency of photovoltaics based on CdSe nanorods and poly(3-hexylthiophene) nanofibers, Physical Chemistry Chemical Physics 8 (2006) 3557–3560.
[101] Y. Wu, G. Zhang, Performance enhancement of hybrid solar cells through chemical vapor annealing, Nano Letters 10 (2010) 1628–1631.
[102] P. Wang, A. Abrusci, H.M.P. Wong, M. Svensson, M.R. Andersson, N.C. Greenham, Photoinduced charge transfer and efficient solar energy conversion in a blend of a red polyfluorene copolymer with CdSe nanoparticles, Nano Letters 6 (2006) 1789–1793.
[103] B. Sun, H.J. Snaith, A.S. Dhoot, S. Westenhoff, N.C. Greenham, Vertically segregated hybrid blends for photovoltaic devices with improved efficiency, Journal of Applied Physics 97 (2005) 014914–014916.
[104] I. Gur, N.A. Fromer, C.-P. Chen, A.G. Kanaras, A.P. Alivisatos, Hybrid solar cells with prescribed nanoscale morphologies based on hyperbranched semiconductor nanocrystals, Nano Letters 7 (2006) 409–414.
[105] Y. Zhou, F.S. Riehle, Y. Yuan, H.-F. Schleiermacher, M. Niggemann, G.A. Urban, M. Kruger, Improved efficiency of hybrid solar cells based on non-ligand-exchanged CdSe quantum dots and poly(3-hexylthiophene), Applied Physics Letters 96 (2010) 013304-013303.
[106] N. Radychev, I. Lokteva, F. Witt, J. Kolny-Olesiak, H. Borchert, J.r. Parisi, Physical origin of the impact of different nanocrystal surface modifications on the performance of CdSe/P3HT hybrid solar cells, The Journal of Physical Chemistry C 115 (2011) 14111–14122.
[107] M.J. Greaney, S. Das, D.H. Webber, S.E. Bradforth, R.L. Brutchey, Improving open circuit potential in hybrid P3HT:CdSe bulk heterojunction solar cells via colloidal tert-butylthiol ligand exchange, ACS Nano 6 (2012) 4222–4230.
[108] J. Yang, A. Tang, R. Zhou, J. Xue, Effects of nanocrystal size and device aging on performance of hybrid poly(3-hexylthiophene):CdSe nanocrystal solar cells, Solar Energy Materials and Solar Cells 95 (2011) 476–482.
[109] J.D. Olson, G.P. Gray, S.A. Carter, Optimizing hybrid photovoltaics through annealing and ligand choice, Solar Energy Materials and Solar Cells 93 (2009) 519–523.
[110] W.U. Huynh, J.J. Dittmer, A.P. Alivisatos, Hybrid nanorod-polymer solar cells, Science 295 (2002) 2425–2427.
[111] J.Y. Lek, L. Xi, B.E. Kardynal, L.H. Wong, Y.M. Lam, Understanding the effect of surface chemistry on charge generation and transport in poly (3-hexylthiophene)/CdSe hybrid solar cells, ACS Applied Materials & Interfaces 3 (2011) 287–292.
[112] W. Yu, H. Zhang, Z. Fan, J. Zhang, H. Wei, D. Zhou, B. Xu, F. Li, W. Tian, B. Yang, Efficient polymer/nanocrystal hybrid solar cells fabricated from aqueous materials, Energy & Environmental Science 112 (2011) 2831–2834.
[113] Y. Kang, Hybrid solar cells with vertically aligned CdTe nanorods and a conjugated polymer, Applied Physics Letters 86 (2005) 113101.
[114] Z. Fan, H. Zhang, W. Yu, Z. Xing, H. Wei, Q. Dong, W. Tian, B. Yang, Aqueous-solution-processed hybrid solar cells from Poly(1,4-naphthalenevinylene) and CdTe nanocrystals, ACS Applied Materials & Interfaces 3 (2011) 2919–2923.
[115] Y.-Y. Yu, W.-C. Chien, Y.-H. Ko, S.-H. Chen, Preparation and characterization of P3HT:CuInSe2:TiO2 thin film for hybrid solar cell applications, Thin Solid Films 520 (2011) 1503–1510.
[116] J. Chen, F. Xu, J. Wu, K. Qasim, Y. Zhou, W. Lei, L.-T. Sun, Y. Zhang, Flexible photovoltaic cells based on a graphene-CdSe quantum dot nanocomposite, Nanoscale 4 (2012) 441–443.
[117] A.R.W. Andrew, B. David, H.W. Jamie, A.T. Elizabeth, L.T. Eric, R.-D. Halina, M. Paul, Lead sulfide nanocrystal: conducting polymer solar cells, Journal of Physics D: Applied Physics, 38 (2005) 2006.
[118] S. Günes, K.P. Fritz, H. Neugebauer, N.S. Sariciftci, S. Kumar, G.D. Scholes, Hybrid solar cells using PbS nanoparticles, Solar Energy Materials and Solar Cells 91 (2007) 420–423.
[119] H.-J. Syu, S.-C. Shiu, C.-F. Lin, Silicon nanowire/organic hybrid solar cell with efficiency of 8.40%, Solar Energy Materials and Solar Cells 98 (2012) 267–272.
[120] S.-C. Shiu, J.-J. Chao, S.-C. Hung, C.-L. Yeh, C.-F. Lin, Morphology dependence of silicon nanowire/poly(3,4-ethylenedioxythiophene):poly(styrenesulfonate) heterojunction solar cells, Chemistry of Materials 22 (2010) 3108–3113.
[121] S.-H. Tsai, H.-C. Chang, H.-H. Wang, S.-Y. Chen, C.-A. Lin, S.-A. Chen, Y.-L. Chueh, J.-H. He, Significant efficiency enhancement of hybrid solar cells using core–shell nanowire geometry for energy harvesting, ACS Nano 5 (2011) 9501–9510.
[122] J.-S. Huang, C.-Y. Hsiao, S.-J. Syu, J.-J. Chao, C.-F. Lin, Well-aligned single-crystalline silicon nanowire hybrid solar cells on glass, Solar Energy Materials and Solar Cells 93 (2009) 621–624.
[123] A. Abrusci, I.K. Ding, M. Al-Hashimi, T. Segal-Peretz, M.D. McGehee, M. Heeney, G.L. Frey, H.J. Snaith, Facile infiltration of semiconducting polymer into mesoporous electrodes for hybrid solar cells, Energy & Environmental Science 4 (2011) 3051–3058.
[124] Y.-Y. Lin, T.-H. Chu, S.-S. Li, C.-H. Chuang, C.-H. Chang, W.-F. Su, C.-P. Chang, M.-W. Chu, C.-W. Chen, Interfacial nanostructuring on the performance of polymer/TiO_2 nanorod bulk heterojunction solar cells, Journal of the American Chemical Society 131 (2009) 3644–3649.
[125] M.-C. Wu, C.-H. Chang, H.-H. Lo, Y.-S. Lin, Y.-Y. Lin, W.-C. Yen, W.-F. Su, Y.-F. Chen, C.-W. Chen, Nanoscale morphology and performance of molecular-weight-dependent poly(3-hexylthiophene)/TiO_2 nanorod hybrid solar cells, Journal of Materials Chemistry 18 (2008) 4097–4102.
[126] J. Lee, J.Y. Jho, Fabrication of highly ordered and vertically oriented TiO_2 nanotube arrays for ordered heterojunction polymer/inorganic hybrid solar cell, Solar Energy Materials and Solar Cells 95 (2011) 3152–3156.
[127] W.J.E. Beek, M.M. Wienk, M. Kemerink, X. Yang, R.A.J. Janssen, Hybrid zinc oxide conjugated polymer bulk heterojunction solar cells, The Journal of Physical Chemistry B 109 (2005) 9505–9516.
[128] H.R. Tan, X.W. Zhang, F.R. Tan, H.L. Gao, Z.G. Yin, Y.M. Bai, X.L. Zhang, S.C. Qu, Performance improvement of conjugated polymer and ZnO hybrid solar cells using nickel oxide as anode buffer layer, physica status solidi (a) 208 (2011) 2865–2870.
[129] A.L. Briseno, T.W. Holcombe, A.I. Boukai, E.C. Garnett, S.W. Shelton, J.J.M. Fre´chet, P. Yang, Oligo- and polythiophene/ZnO hybrid nanowire solar cells, Nano Letters 10 (2009) 334–340.
[130] E. Kucur, J. Riegler, G.A. Urban, T. Nann, Determination of quantum confinement in CdSe nanocrystals by cyclic voltammetry, The Journal of Chemical Physics 119 (2003) 2333–2337.
[131] D. Herrmann, S. Niesar, C. Scharsich, A. Köhler, M. Stutzmann, E. Riedle, Role of structural order and excess energy on ultrafast free charge generation in hybrid polythiophene/Si photovoltaics probed in real time by near-infrared broadband transient absorption, Journal of the American Chemical Society 133 (2011) 18220–18233.
[132] J. Derr, K. Dunn, D. Riabinina, F. Martin, M. Chaker, F. Rosei, Quantum confinement regime in silicon nanocrystals, Physica E: Low-dimensional Systems and Nanostructures 41 (2009) 668–670.
[133] T. van Buuren, L.N. Dinh, L.L. Chase, W.J. Siekhaus, L.J. Terminello, Changes in the electronic properties of Si nanocrystals as a function of particle size, Physical Review Letters 80 (1998) 3803–3806.
[134] M. Lira-Cantu, A. Chafiq, J. Faissat, I. Gonzalez-Valls, Y. Yu, Oxide/polymer interfaces for hybrid and organic solar cells: anatase vs, Rutile TiO_2, Solar Energy Materials and Solar Cells 95 (2011) 1362–1374.
[135] J. Huang, Z. Yin, Q. Zheng, Applications of ZnO in organic and hybrid solar cells, Energy & Environmental Science 4 (2011) 3861–3877.
[136] J. Weickert, R.B. Dunbar, H.C. Hesse, W. Wiedemann, L. Schmidt-Mende, Nanostructured organic and hybrid solar cells, Advanced Materials 23 (2011) 1810–1828.
[137] B. O'Regan, M. Gratzel, A low-cost, high efficiency solar cell based on dye-sensitised colloidal TiO_2 films, Nature 353 (1991) 737–740.
[138] W. Jih-Jen, C. Guan-Ren, L. Chia-Chun, W. Wei-Ting, C. Jen-Sue, Performance and electron transport properties of TiO_2 nanocomposite dye-sensitized solar cells, Nanotechnology 19 (2008) 105702.
[139] J.-H. Yum, P. Chen, M. Grätzel, M.K. Nazeeruddin, Recent developments in solid-state dye-sensitized solar cells, ChemSusChem 1 (2008) 699–707.
[140] M. Grätzel, Dye-sensitized solid-state heterojunction solar cells, MRS Bulletin 30 (2005).
[141] N. Tetreault, M. Gratzel, Novel nanostructures for next generation dye-sensitized solar cells, Energy & Environmental Science, (2012). 10.1039/C2EE03242B.
[142] G.K. Mor, K. Shankar, M. Paulose, O.K. Varghese, C.A. Grimes, High efficiency double heterojunction polymer photovoltaic cells using highly ordered TiO_2 nanotube arrays, Applied Physics Letters 91 (2007) 152111–152113.
[143] T.R.B. Foong, K.L. Chan, X. Hu, Structure and properties of nano-confined poly(3-hexylthiophene) in nano-array/polymer hybrid ordered-bulk heterojunction solar cells, Nanoscale 4 (2012) 478–485.
[144] S. Shao, J. Liu, B. Zhang, Z. Xie, L. Wang, Enhanced stability of zinc oxide-based hybrid polymer solar cells by manipulating ultraviolet light distribution in the active layer, Applied Physics Letters 98 (2011) 203304-203303.
[145] R. Kroon, M. Lenes, J.C. Hummelen, P.W.M. Blom, B. de Boer, Small Bandgap polymers for organic solar cells (polymer material development in the last 5 years), Polymer Reviews 48 (2008) 531–582.
[146] G. Martin A, Third generation photovoltaics: solar cells for 2020 and beyond, Physica E: Low-dimensional Systems and Nanostructures 14 (2002) 65–70.
[147] S.A. McDonald, G. Konstantatos, S. Zhang, P.W. Cyr, E.J.D. Klem, L. Levina, E.H. Sargent, Solution-processed PbS quantum dot infrared photodetectors and photovoltaics, Nature Materials 4 (2005) 138–142.
[148] N. Arthur J, Multiple exciton generation in semiconductor quantum dots, Chemical Physics Letters 457 (2008) 3–11.
[149] R.J. Ellingson, M.C. Beard, J.C. Johnson, P. Yu, O.I. Micic, A.J. Nozik, A. Shabaev, A.L. Efros, Highly efficient multiple exciton generation in colloidal PbSe and PbS quantum dots, Nano Letters 5 (2005) 865–871.

[150] M.C. Beard, K.P. Knutsen, P. Yu, J.M. Luther, Q. Song, W.K. Metzger, R.J. Ellingson, A.J. Nozik, Multiple exciton generation in colloidal silicon nanocrystals, Nano Letters 7 (2007) 2506–2512.
[151] O.E. Semonin, J.M. Luther, S. Choi, H.-Y. Chen, J. Gao, A.J. Nozik, M.C. Beard, Peak external photocurrent quantum efficiency exceeding 100% via MEG in a quantum dot solar cell, Science 334 (2011) 1530–1533.
[152] W.W. Yu, Y.A. Wang, X. Peng, Formation and stability of size-, shape-, and structure-controlled CdTe nanocrystals: ligand effects on monomers and nanocrystals, Chemistry of Materials 15 (2003) 4300–4308.
[153] C. Goh, S.R. Scully, M.D. McGehee, Effects of molecular interface modification in hybrid organic–inorganic photovoltaic cells, Journal of Applied Physics 101 (2007) 114503–114512.
[154] I. Lokteva, N. Radychev, F. Witt, H. Borchert, J.r. Parisi, J. Kolny-Olesiak, Surface treatment of CdSe nanoparticles for application in hybrid solar cells: the effect of multiple ligand exchange with pyridine, The Journal of Physical Chemistry C 114 (2010) 12784–12791.
[155] W.U. Huynh, J.J. Dittmer, W.C. Libby, G.L. Whiting, A.P. Alivisatos, Controlling the morphology of nanocrystal–polymer composites for solar cells, Advanced Functional Materials 13 (2003) 73–79.
[156] L.X. Reynolds, T. Lutz, S. Dowland, A. MacLachlan, S. King, S.A. Haque, Charge photogeneration in hybrid solar cells: a comparison between quantum dots and *in situ* grown CdS, Nanoscale 4 (2012) 1561–1564.
[157] C.R. McNeill, Morphology of all-polymer solar cells, Energy & Environmental Science 5 (2012) 5653–5667.
[158] H. Hoppe, N.S. Sariciftci, Morphology of polymer/fullerene bulk heterojunction solar cells, Journal of Materials Chemistry 16 (2006) 45–61.
[159] H. Sirringhaus, P.J. Brown, R.H. Friend, M.M. Nielsen, K. Bechgaard, B.M.W. Langeveld-Voss, A.J.H. Spiering, R.A.J. Janssen, E.W. Meijer, P. Herwig, D.M. de Leeuw, Two-dimensional charge transport in self-organized, high-mobility conjugated polymers, Nature 401 (1999) 685–688.
[160] P. Schilinsky, U. Asawapirom, U. Scherf, M. Biele, C.J. Brabec, Influence of the molecular weight of poly(3-hexylthiophene) on the performance of bulk heterojunction solar cells, Chemistry of Materials 17 (2005) 2175–2180.
[161] M.S. Ryu, H.J. Cha, J. Jang, Effects of thermal annealing of polymer:fullerene photovoltaic solar cells for high efficiency, Current Applied Physics 10 (2010) S206–S209.
[162] T.M. Clarke, F.C. Jamieson, J.R. Durrant, Transient absorption studies of bimolecular recombination dynamics in polythiophene/fullerene blend films, The Journal of Physical Chemistry C 113 (2009) 20934–20941.
[163] I.A. Howard, F. Laquai, Optical probes of charge generation and recombination in bulk heterojunction organic solar cells, Macromolecular Chemistry and Physics 211 (2010) 2063–2070.
[164] O. Douhéret, A. Swinnen, S. Bertho, I. Haeldermans, J. D'Haen, M. D'Olieslaeger, D. Vanderzande, J.V. Manca, High-resolution morphological and electrical characterisation of organic bulk heterojunction solar cells by scanning probe microscopy, Progress in Photovoltaics: Research and Applications 15 (2007) 713–726.
[165] M. Dante, J. Peet, T.-Q. Nguyen, Nanoscale charge transport and internal structure of bulk heterojunction conjugated polymer/fullerene solar cells by scanning probe microscopy, The Journal of Physical Chemistry C 112 (2008) 7241–7249.
[166] S.S.v. Bavel, E. Sourty, G.d. With, J. Loos, Three-dimensional nanoscale organization of bulk heterojunction polymer solar cells, Nano Letters 9 (2008) 507–513.
[167] H. Hoppe, T. Glatzel, M. Niggemann, A. Hinsch, M.C. Lux-Steiner, N.S. Sariciftci, Kelvin Probe Force, Microscopy study on conjugated polymer/fullerene bulk heterojunction organic solar cells, Nano Letters 5 (2005) 269–274.
[168] L.S.C. Pingree, O.G. Reid, D.S. Ginger, Electrical scanning probe microscopy on active organic electronic devices, Advanced Materials 21 (2009) 19–28.
[169] V. Palermo, M. Palma, P. Samorì, Electronic characterization of organic thin films by kelvin probe force microscopy, Advanced Materials 18 (2006) 145–164.
[170] M. Saint Jean, S. Hudlet, C. Guthmann, J. Berger, Charge dynamics and time evolution of contact potential studied by atomic force microscopy, Physical Review B 56 (1997) 15391–15395.
[171] B. Azzopardi, C.J.M. Emmott, A. Urbina, F.C. Krebs, J. Mutale, J. Nelson, Economic assessment of solar electricity production from organic-based photovoltaic modules in a domestic environment, Energy & Environmental Science 4 (2011) 3741–3753.
[172] F.C. Krebs, T. Tromholt, M. Jorgensen, Upscaling of polymer solar cell fabrication using full roll-to-roll processing, Nanoscale 2 (2010) 873–886.
[173] F.C. Krebs, S.A. Gevorgyan, J. Alstrup, A roll-to-roll process to flexible polymer solar cells: model studies, manufacture and operational stability studies, Journal of Materials Chemistry 19 (2009) 5442–5451.
[174] R. Dunford, A. Salinaro, L. Cai, N. Serpone, S. Horikoshi, H. Hidaka, J. Knowland, Chemical oxidation and DNA damage catalysed by inorganic sunscreen ingredients, FEBS Letters 418 (1997) 87–90.
[175] L. Reijnders, Human health hazards of persistent inorganic and carbon nanoparticles, Journal of Materials Science 47 (2012) 5061–5073.
[176] R. Sondergaard, M. Hosel, D. Angmo, T.T. Larsen-Olsen, F.C. Krebs, Roll-to-roll fabrication of polymer solar cells, Materials Today 15 (2012) 36–49.
[177] Q. Dong, W. Yu, Z. Li, S. Yao, X. Zhang, B. Yang, C. Im, W. Tian, All-water-solution processed solar cells based on PPV and TiO2 nanocrystals, Solar Energy Materials and Solar Cells 104 (2012) 75–80.
[178] V. Fthenakis, Sustainability of photovoltaics: the case for thin-film solar cells, Renewable and Sustainable Energy Reviews 13 (2009) 2746–2750.
[179] C.A. Wolden, J. Kurtin, J.B. Baxter, I. Repins, S.E. Shaheen, J.T. Torvik, A.A. Rockett, V.M. Fthenakis, E.S. Aydil, Photovoltaic manufacturing: present status, future prospects, and research needs, Journal of Vacuum Science & Technology A: Vacuum, Surfaces, and Films 29 (2011) 030801–030816.
[180] 〈http://minerals.usgs.gov/minerals/pubs/mcs/2012/mcs2012.pdf〉.
[181] F.C. Krebs, Roll-to-roll fabrication of monolithic large-area polymer solar cells free from indium-tin-oxide, Solar Energy Materials and Solar Cells 93 (2009) 1636–1641.
[182] F.C. Krebs, All solution roll-to-roll processed polymer solar cells free from indium-tin-oxide and vacuum coating steps, Organic Electronics 10 (2009) 761–768.
[183] M. Jørgensen, K. Norrman, S.A. Gevorgyan, T. Tromholt, B. Andreasen, F.C. Krebs, Stability of polymer solar cells, Advanced Materials 24 (2012) 580–612.
[184] X. Yang, J.K.J. van Duren, R.A.J. Janssen, M.A.J. Michels, J. Loos, Morphology and thermal stability of the active layer in poly(p-phenylenevinylene)/methanofullerene plastic photovoltaic devices, Macromolecules 37 (2004) 2151–2158.
[185] J. Yang, L. Qian, R. Zhou, Y. Zheng, A. Tang, P.H. Holloway, J. Xue, Hybrid polymer:colloidal nanoparticle photovoltaic cells incorporating a solution-processed, multi-functioned ZnO nanocrystal layer, Journal of Applied Physics 111 (2012) 044323–044328.
[186] M.M. Voigt, R.C.I. Mackenzie, S.P. King, C.P. Yau, P. Atienzar, J. Dane, P.E. Keivanidis, I. Zadrazil, D.D.C. Bradley, J. Nelson, Gravure printing inverted organic solar cells: the influence of ink properties on film quality and device performance, Solar Energy Materials and Solar Cells 105 (2012) 77–85.
[187] L. Wengeler, B. Schmidt-Hansberg, K. Peters, P. Scharfer, W. Schabel, Investigations on knife and slot die coating and processing of polymer nanoparticle films for hybrid polymer solar cells, Chemical Engineering and Processing: Process Intensification 50 (2011) 478–482.
[188] R. García-Valverde, J.A. Cherni, A. Urbina, Life cycle analysis of organic photovoltaic technologies, Progress in Photovoltaics: Research and Applications 18 (2010) 535–558.
[189] N. Espinosa, R. García-Valverde, A. Urbina, F.C. Krebs, A life cycle analysis of polymer solar cell modules prepared using roll-to-roll methods under ambient conditions, Solar Energy Materials and Solar Cells 95 (2011) 1293–1302.
[190] B. Azzopardi, J. Mutale, Life cycle analysis for future photovoltaic systems using hybrid solar cells, Renewable and Sustainable Energy Reviews 14 (2010) 1130–1134.